Vortex Induced Vibration Energy Harvesting through Piezoelectric Transducers

A Major Qualifying Project

Submitted to the Faculty of the

WORCESTER POLYTECHNIC INSTITUTE

In partial fulfillment of the requirements for the

Degree of Bachelor of Science

Submitted By:

Natalie Diltz

Julie Gagnon

Jacqueline O'Connor

Jessica Wedell

Project Advisor:

Professor Brian J. Savilonis

Submitted:

4/20/2017

Abstract

Harvesting energy from vortex induced vibrations (VIV) in flowing water has the potential to be a low-impact, low-cost alternative to traditional hydropower methods. This project focused on utilizing piezoelectric transducers to transform the VIV oscillations of a cylinder to electrical power. Initial prototypes focused on achieving these oscillations. The final prototype of this stage produced an average amplitude of 12mm and frequency of 3.2 Hz. These values were used to determine the design of the piezoelectric system. The second stage of prototyping focused on generating power through the integration of the existing prototype and the piezoelectric transducers. The final prototype successfully produced up to 0.1 microwatts, but the erratic flow speed of the testing facilities and the project's small scale prevented consistent power generation. The project concluded that additional experimentation needs to be conducted on a larger scale in order to determine the real world feasibility of VIV piezoelectric energy harvesting.

Table of Contents

List of Figures

List of Tables

1. Introduction

The production of clean, renewable energy is one of the biggest challenges faced by the world today. Currently, the United States generates approximately 90% of its energy from nonrenewable sources such as coal, natural gas, and oil. These resources are being drained at an unsustainable rate and are the leading contributors to environmental problems such as pollution and global warming. In recent decades, geothermal, wind, solar, biomass, and hydropower have been explored as renewable energy sources. However, these energy sources still only make up about 10% of US energy consumption because they are more expensive and require larger amounts of land than their non-renewable counterparts (US Energy Information Administration).

Currently, hydropower accounts for 46% of renewable energy in the US. Hydropower is a particularly promising field because rivers and oceans make up about 71% of Earth's surface area. In spite of that promise, many of the current methods of harnessing hydropower energy have significant drawbacks. Hydropower dams are the most commonly used method due to the amount of power they can produce. However, they can only be built on large rivers with large flow rates, which limits accessibility to this type of power. Additionally, dams can have significant negative impacts on river ecosystems and wildlife. Other common methods of hydropower production include wave generators and underwater turbines. While these methods have potential, wave generators are limited in location because they disrupt surface marine transit and turbines are limited to rivers with a current of at least 2 m/s.

A new type of hydropower energy harvests the power of vortex induced vibrations (VIV). VIV is a phenomenon that occurs when a bluff body is placed in a flowing fluid; a shear layer forms on either side of the body, and as the shear layers separate, they curl back behind the body forming a pattern of alternating vortices. These vortices exert an oscillatory lift force on the body, causing it to vibrate up and down. These vibrations can then be harvested as electrical power. VIV has several advantages over other hydropower methods. For one, VIV can be used in flow speeds ranging from 0.2 to 2.5 m/s. This versatility means that VIV has the potential to be used in low current applications and along coastlines. In addition, VIV devices are more environmentally friendly because they cause minimal damage or alterations to ecosystems and do not interrupt marine traffic.

While VIV has many benefits, it is currently not commercially utilized as a form of power generation. One of the main challenges of utilizing VIV is determining how to maximize the power that can be harvested from the oscillations. Significant research has been done on how to maximize the amplitude and frequency of the vibrations. Previous MQPs investigated changing the size, material, and dimensions of the oscillating body. However, there is still need for further research into how to effectively use VIV to generate power.

The goal of this project was to construct a VIV energy harvester that converts the oscillations of a cylinder into electrical power through the use of piezoelectric transducers. The harvester was tested in flowing water and optimal electrical load resistance testing was conducted outside the water. The VIV harvester was able to produce 0.1μW of power in the flowing water. However, continuous oscillation proved difficult because of inconsistent flow speed of the testing location. It was concluded that additional testing needs to be conducted in order to ascertain the viability of piezoelectric VIV energy harvesting.

2. Background

The purpose of this chapter is to introduce vortex induced vibrations, its applications, past research, and methods of energy harvesting. The following section describes the theory behind vortex shedding and vortex induced vibrations as well as some of the parameters and equations that can be used to characterize it. Section 2.2 discusses some of the benefits and applications of VIV, particularly as it relates to energy harvesting. Section 2.3 presents some of the previous research that has been done in this field, including past MQPs at WPI and the VIVACE converter developed at the University of Michigan. Finally, Section 2.4 examines different methods of energy harvesting and energy conversion. This section also discusses the theory behind maximizing power through changing the load on a device.

2.1 VIV Theory

2.1.1 Vortex Shedding

Vortex shedding is a phenomenon that occurs as the result of a viscous fluid flowing over a bluff body, such as a cylinder, which causes a boundary layer to form due to the shear viscosity of the fluid. As the fluid flows over the bluff body, the boundary layers separate and form two separate shear layers trailing behind the body (Bearman, 196). The fluid closer to the body, which is in contact with the wake, moves slower than the fluid near the outer edges of the shear layer, which is in contact with the free stream. As a result, in the near wake of the body, the fluid rotates inwards, forming distinct vortices that are shed from the body and travel down the wake (Blevins, 45).

The vortices on each side of the bluff body are opposite in sign and will form a regular periodic pattern in the wake known as a vortex street. The formation of a vortex street was examined by Theodore von Kármán, who developed a model for an ideal vortex street (Figure 1). He found that the ideal spacing for a vortex street was $h/l = 0.281$, where h is the vertical distance between vortices, and l is the horizontal distance between vortices (Blevins, 46).

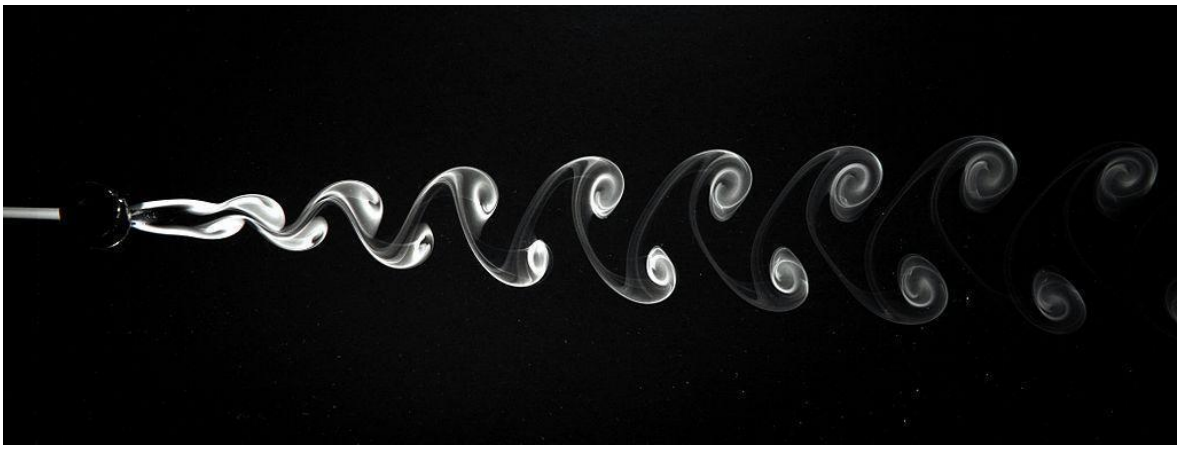

Figure 1: A Von Kármán Vortex Street (Jürgen Wagner)

Vortex street formation is highly dependent on Reynolds number, which is defined as the ratio of inertial forces to viscous forces. The Reynolds number (Equation 1) is a dimensionless parameter that depends on the fluid velocity (U), the characteristic length of the body (D), and the kinematic viscosity of the fluid (ν).

$$Re = \frac{UD}{\nu}$$

Equation 1

The Reynold's number regimes that affect the vortex shedding of a cylinder are summarized in Figure 2 below.

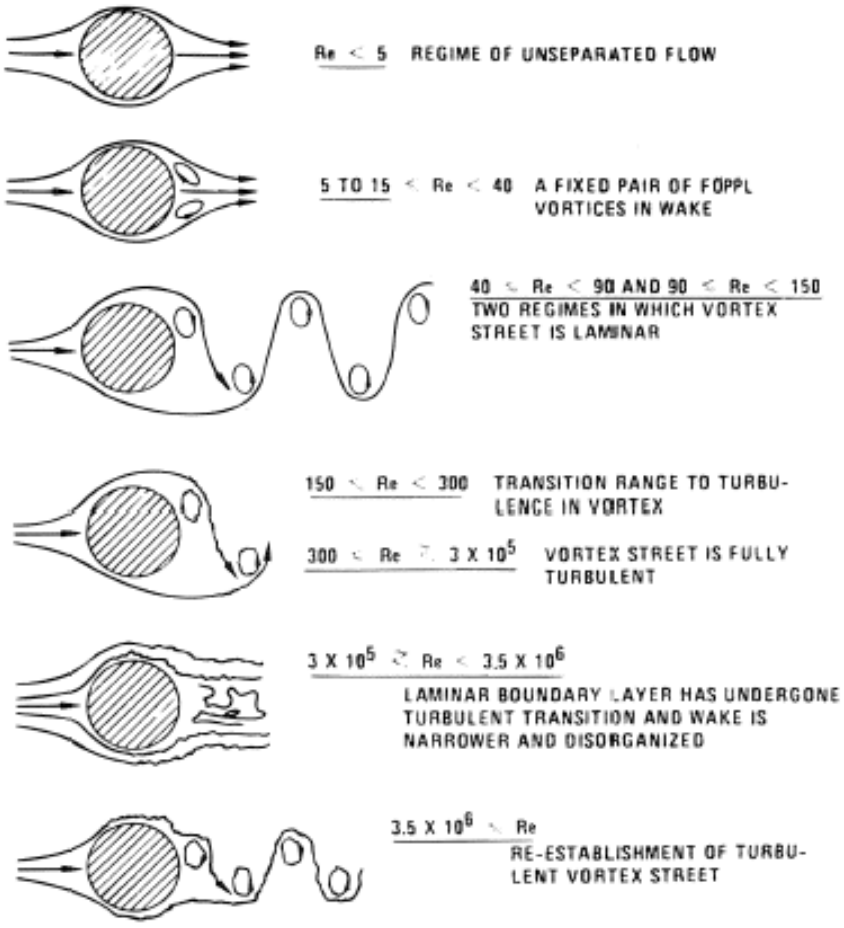

Figure 2: Reynolds Number Regimes for Fluid Flow across Smooth Cylinders (Lienhard, 1966)

Below Re=5, the flow follows the contour of the cylinder and no vortices are formed. From $5 \leq Re \leq 40$, the flow separates behind the cylinder, and a pair of symmetric vortices form. As the Reynolds number increases, one of the vortices breaks away, triggering the formation of a vortex street. From $40 \leq Re \leq 150$ a laminar vortex street forms in the wake. Over the next range of Reynolds numbers from $150 \leq Re \leq 300$, the vortices become turbulent, even though the boundary layer and free stream are still laminar. In this transition region, there is no organized shedding or lift force. From $300 \leq Re \leq 3x10^5$, there is strong periodic shedding, which produces a vortex street that is fully turbulent and stable. This is the range of Reynold's numbers in which most VIV experiments have been conducted, as it produces the most stable vortex streets and lift forces. As the Reynold's number increases past $3x10^5$, the boundary layer becomes turbulent, and the wake becomes disorganized and unpredictable. At some point around a Reynolds number of $3.5x10^6$, vortex shedding resumes with a turbulent boundary

layer. Vortex shedding has been observed at Reynolds numbers as high as 10^{11}, such as in wind-driven cloud formations (Blevins, 46).

2.1.2 Vortex Induced Vibration

The vortices shed from bluff bodies exert oscillatory lift forces on the body due to alternating pressures. If the body is flexible or unfixed, these forces will cause it to oscillate as well (Benaroya & Gabbai). The oscillation of bluff bodies due to vortex shedding is known as vortex induced vibration (VIV). While VIV can occur for any bluff body, this report will focus on the vortex induced vibration of cylinders. The oscillations mostly occur in the direction normal to the free stream, and cylinders can have oscillation amplitudes up to about twice the size of the cylinder diameter (Bearman, 195).

2.1.3 Important Parameters

The vortex induced vibration of a cylinder is dependent on several key parameters. The first important parameter is the Reynolds number. The Reynolds number, as discussed previously, affects the vortex shedding pattern of the flow, meaning that VIV will only occur in Reynolds regimes where there is a stable vortex street. For most VIV applications, this means that Reynold's number will be between 300 and $3x10^5$.

The Strouhal number is another dimensionless parameter that is significant in VIV because it characterizes oscillating flow mechanisms (Equation 2),

$$S = \frac{f_s D}{U}$$

Equation 2

where S is the Strouhal number, D is the diameter of the cylinder, and f_s is the vortex shedding frequency [Hz]. The Strouhal number for a cylinder is a function of the Reynolds number, the surface roughness, and the free stream turbulence (Figure 3). Over the regime of Reynolds numbers from $300 \leq Re \leq 3x10^5$, the Strouhal number is nearly constant at a value of 0.2 (Benaroya & Gabbai). Taking the Strouhal number to be constant is useful for simplifying equations, because it makes the vortex shedding frequency a function of only the flow speed and the cylinder diameter.

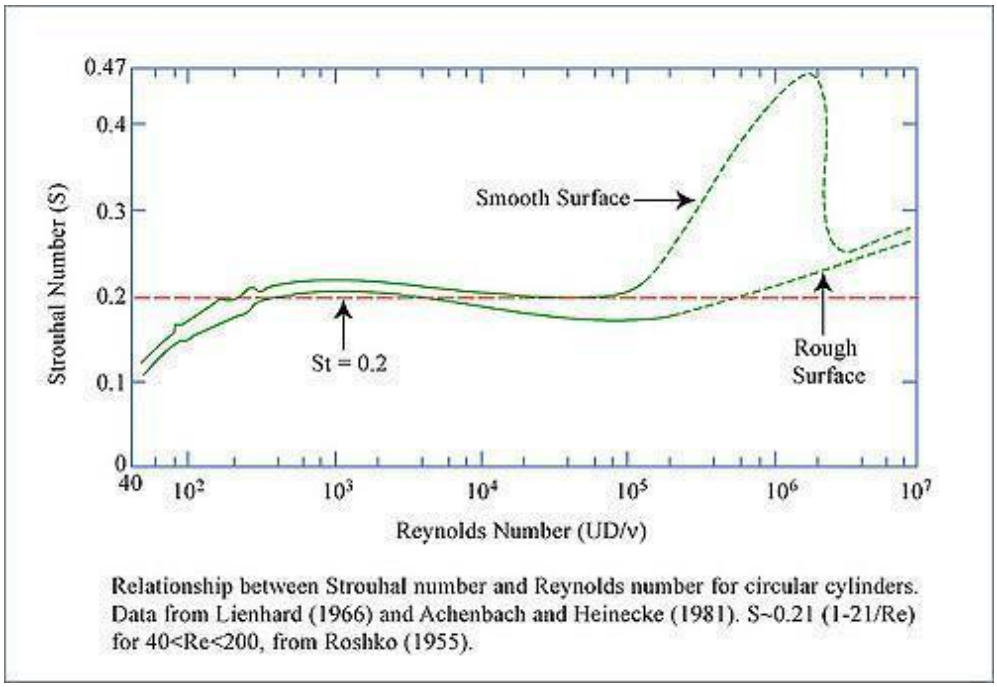

Figure 3: Graph Showing the Relationship between the Strouhal and Reynolds Numbers for a Cylinder (MIT)

A third parameter that affects vortex induced vibration is the mass ratio (m*). The mass ratio is the ratio of the oscillator mass to the mass of the fluid it displaces (Equation 3).

$$m^* = \frac{m_{osc}}{m_{dis}}$$

Equation 3

m_{osc} is the mass of the oscillating body plus ⅓ the total mass of the springs, and m_{dis} is the mass of the fluid displaced by the cylinder. For a cylinder:

$$m_{dis} = \rho \frac{\pi}{4} D^2 L$$

Equation 4

D is the diameter of the cylinder, L is the length of the cylinder, and ρ is the density of the fluid. Excluding the mass of the springs and any additional sources of mass attached to the cylinder, the mass ratio reduces to the ratio between the density of the cylinder and the density of the fluid (Modir, Kahrom, & Farshidianfar).

Two additional significant parameters of VIV are the structural damping factor or damping ratio (ζ) and the aspect ratio of the cylinder (L/D). The damping factor is on a scale of

0 to 1, with one being the critical damping factor for the system. The critical damping is the point at which the system of a damped oscillator goes from being underdamped to overdamped, i.e. where the cylinder can no longer vibrate. The damping of a system is often characterized by a dimensionless parameter called reduced damping, such as the Scruton number (Equation 5).

$$Sc = \frac{2m(2\pi\zeta)}{\rho D^2}$$

Equation 5

D is the diameter of the cylinder, m is the mass of the cylinder per unit length, ρ is the density of the fluid and ζ is the damping ratio. Increasing the reduced damping usually decreases the amplitude of oscillations (Blevins, 9). Damping on the cylinder is the result of viscous forces, which include the drag on the cylinder and the friction due to how the cylinder is mounted. The drag force on the cylinder is not linear; it depends on the amplitude and reduced velocity of the cylinder. Studies have attempted to model the damping ratio as a function of time. However, most calculations assume an average value. The damping ratio for freely-suspended cylinders is typically very low, on the scale of 0.06 or less. Any constraints on the cylinder where there is friction will increase the damping on the system (Williamson & Govardhan, 2008). The average damping for the system can be determined by performing a free decay test at a given starting amplitude and measuring two consecutive amplitudes of the cylinder (Modir, Kahrom, & Farshidianfar). The damping ratio is then calculated as follows, where y_n is the first amplitude and y_{n+1} is the second amplitude:

$$\zeta = \frac{1}{2\pi} \ln \frac{y_n}{y_{n+1}}$$

Equation 6

There are two more dimensionless parameters that are useful in characterizing the oscillations of a system undergoing VIV. The first of these parameters is the reduced velocity (U*) (Equation 7).

$$U^* = \frac{U}{f_n D}$$

Equation 7

U is the fluid velocity, f_n is the natural frequency of the system, and D is the diameter of the cylinder. The final significant dimension parameter of VIV is the dimensionless amplitude, which is defined as the ratio of the amplitude of the vibrations in the transverse direction to the diameter of the cylinder (Blevins, 5).

2.1.4 Synchronization

A key feature of vortex induced vibration is the existence of a region of synchronization or "lock-in." In this region, there is a significant increase in the amplitude of the oscillations of the cylinder, meaning that the energy of the system will be at a maximum. Synchronization is similar to linear resonance, as it occurs when the vortex shedding frequency approaches the natural frequency of the oscillator. However, unlike resonance, synchronization is nonlinear and will occur over a band of frequencies. Additionally, synchronization does not have a sharp peak in amplitude when the shedding frequency and the natural frequency are exactly equal. In the lock-in region, the vibration of the cylinder controls the shedding frequency. Synchronization is also described as being self-limiting, because when the amplitude grows too large the symmetric pattern of vortices breaks up (Blevins, 54).

Most of the current understanding of lock-in is based on empirical or semi-empirical studies; an analytical model of lock-in has not been fully developed. One of the most important findings about the lock-in region is its dependence on the reduced velocity. Assuming a value of 0.2 for the Strouhal number, the reduced velocity, U*, is equal to 5 when the vortex shedding frequency and the natural frequency are exactly equal. It has been experimentally determined that synchronization will generally occur for 4< U* <8 (Blevins, 59).

While the reduced velocity is the best indicator of whether or not synchronization will occur, it has also been found that the mass ratio affects the size of the lock-in region. For high values of m*, the lock-in region is relatively constant between reduced velocities of 4 and 8. As the mass ratio is decreased, the lock-in region becomes larger, until it reaches a critical point where the lock-in band becomes infinitely large. Williamson and Govordhan found that this critical mass ratio was equal to 0.54. This value was determined specifically for systems with a low mass and low damping for an elastically supported cylinder. However, the existence of a critical mass has been demonstrated for different geometries and damping factors. Figure 4 shows the synchronization range as it relates to both m* and U* for a cylinder. Lock-in will

occur within the shaded region.

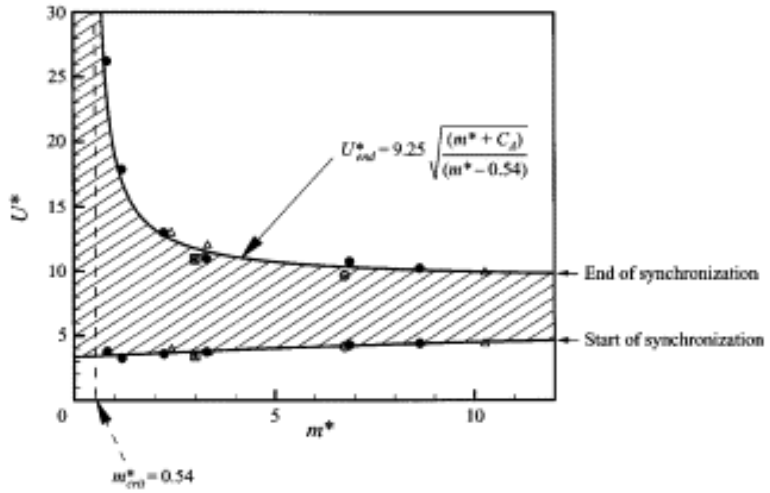

Figure 4: Synchronization Range of a Cylinder as a Function of m* and U* (Williamson & Govordhan)

2.1.5 Harmonic Model of VIV

Due to the variable and non-linear nature of vortex induced vibrations, there is not one set of governing equations to describe it. However, since vortex shedding is approximately sinusoidal, VIV of a cylinder can be reasonably modeled as a linear harmonic oscillator (Blevins, 61). The lift force exerted on the cylinder by the vortex shedding can therefore be modeled as:

$$F_L = \frac{1}{2}\rho U^2 D L C_L \sin(\omega_s t)$$

Equation 8

F_L is the lift force perpendicular to the free stream, ρ is the fluid density, U is the free stream velocity, D is the cylinder diameter, L is the length of the cylinder, t is time [s], and ω_s is the angular vortex shedding frequency [rad/s], where $\omega_s = 2\pi f_s$. This force is applied to a cylinder mounted elastically using springs of combined stiffness k. The motion of the cylinder can then be described by Equation 9 below.

$$m\ddot{y} + 2m\zeta\omega_n\dot{y} + ky = \frac{1}{2}\rho U^2 D L C_L \sin(\omega_s t)$$

Equation 9

ω_n is the angular natural frequency of the cylinder [rad/s], where $\omega_n = 2\pi f_n = \sqrt{\frac{k(1-\zeta^2}{m_{ocs}+m_{dis}}}$, y is the vertical displacement of the cylinder, with the apostrophes signifying differentiation with respect to time, and ζ is the structural damping factor. For the linear oscillator model, the damping factor is taken as an average and assumed to be constant. This differential equation can be solved to produce an equation for the linear displacement of the cylinder with respect to time, where φ is the phase angle:

$$y(t) = \frac{\frac{1}{2}\rho U^2 D L C_L \sin(\omega_s t + \varphi)}{k\sqrt{(1 - \left(\frac{\omega_s}{\omega_n}\right)^2)^2 + (2\zeta\frac{\omega_s}{\omega_n})^2}}$$

Equation 10

From this equation, the amplitude at resonance can be found by setting $\omega_n = \omega_s$:

$$\frac{A}{D} = \frac{\omega_n \rho L U^2 C_L}{4k\zeta}$$

Equation 11

In reality the maximum amplitude will occur over a range of frequencies, not at exact resonance. However, using the linear harmonic oscillator model provides a relatively accurate approximation of the motion of a cylinder undergoing VIV.

The linear harmonic oscillator model of VIV also allows for the theoretical maximum power to be calculated. The velocity as a function of time for the cylinder can be obtained by differentiating Equation 10 for displacement, resulting in the following equation:

$$v(t) = -\frac{\omega_s \frac{1}{2}\rho U^2 D L C_L \cos(\omega_s t + \varphi)}{k\sqrt{(1 - \left(\frac{\omega_s}{\omega_n}\right)^2)^2 + (2\zeta\frac{\omega_s}{\omega_n})^2}}$$

Equation 12

Power as a function of time is found by multiplying the lift force and the cylinder velocity, which gives:

$$P(t) = -\frac{\omega_s \frac{1}{4}\rho^2 U^4 D^2 L^2 {C_L}^2 sin\,(\omega_s t)\, cos\,(\omega_s t + \varphi)}{k\sqrt{(1-(\frac{\omega_s}{\omega_n})^2)^2 + (2\zeta\frac{\omega_s}{\omega_n})^2}}$$

Equation 13

The maximum power will occur when $\omega_n = \omega_s$. Given that for a cylinder $\varphi = \frac{\pi}{2}$, the equation for the maximum power is given as:

$$P_{max} = \frac{\omega_n \rho^2 U^4 D^2 L^2 {C_L}^2 \sin^2(\omega_n t)}{8k\zeta}$$

Equation 14

This equation estimates the system power of a cylinder undergoing VIV. As an example, for a 27.7 mm diameter PVC cylinder that is 229 mm long with a damping ratio of 0.1 suspended by springs with a stiffness of 142.6 N/m in water flowing at 0.5 m/s, the maximum system power is about 0.12 W. For a similar cylinder with a 63.5 mm diameter that is 305 mm long and in water moving at 1m/s, the maximum power increases to 4.03W.

2.2 Applications

VIV is a viable energy source because it can be used in a multitude of environments. VIV devices can be optimized in shape and size for low flow and low head water applications. This ability makes it ideal for streams, small rivers, ocean currents and tidal waves which are abundantly available yet underutilized because they are not dense enough for larger hydropower capabilities. For example, the Gulf Stream moves at a maximum speed of 3 knots (Elert 2002), while most hydropower harvesters require 5-6 knots to work efficiently. VIVACE, a VIV harvesting device designed by University of Michigan engineers, is designed to generate power in water flowing as slow as 2-4 knots. The VIVACE technology would make it possible to harvest energy from the Gulf Stream as well as other river and ocean currents.

Vortex induced vibrations also occur at faster water velocities, making VIV harvesters a highly adaptable energy source. Because of this adaptability, VIV could be used along shorelines at sufficient depth. This is particularly beneficial because over 50% of the US population lives within 50 miles of a coastline, which means there is a large demand for power generation along the coast.

2.2.1. Environmental Factors

Vortex induced vibration devices have definitive advantages over other, more intrusive, hydropower options. A dam, for example, changes the natural orientation of a river, harming plants and wildlife both on land and in water. The most obvious illustration of this is the obstruction of fish migration. While most modern dams are equipped with fish ladders (underwater staircases that help fish navigate around obstacles) or other methods of fish passage, these methods are not always effective and can cause declines in fish populations in these areas ("American Shad", University Communications, 2013).

Large hydropower dams create reservoirs that may flood areas where both humans and wildlife inhabit, which would require relocation. An extreme illustration of this is the Three Gorges Dam on the Yangtze River in China. When the dam was constructed, nearly 1.3 million people were required to relocate since the reservoir would flood their villages (Kuhn, 2008). In addition to these villages, approximately 2,000 archeological sites were also flooded. Some of these sites dated back to the Paleolithic era and included ancient burial grounds (See, 2003).

Wave generators are much less harmful to the environment. Their underwater infrastructure can actually create new habitats for smaller ocean organisms, though it may obstruct larger ocean animals that could become entangled in the structure's cables (OSU, 2015). Wave energy also restricts commercial fishing, creating a virtual marine reserve in their installation area. The major negative side effect of wave generators is the interruption of ship transportation. Due to their low profile and small size, wave generators are difficult to see on the ocean's surface and therefore create navigational hazards to vessels in the area where generators are installed. Additionally, wave generators affect recreation and tourism due to their visual impact and obstruction of activities such as watersports, swimming, and scuba diving ("Environmental Impact of Wave Energy Devices").

VIV devices can be located on the ocean or river floor; therefore they do not impede shipping or recreational activities. Like wave generators, VIV devices would restrict fishing and preserve marine life. However, VIV devices can be small in size and would not obstruct the flow of a river or the transportation of fish. The environment both in and out of water around these devices would remain relatively unchanged. For these reasons, VIV devices present an environmental advantage over more popular, conventional hydropower options.

2.2.2. Cost

VIVACE engineers estimate that when the VIVACE system is deployed it will be able to provide clean energy at 5.5 cents per kilowatt hour, which compares favorably to other forms of clean energy. Wind energy, for example, costs 6.9 cents per kilowatt hour. Solar power can cost anywhere from 16 to 48 cents per kilowatt hour (Flahiff 2008). While the cost of VIV power is just an estimate because there are not currently any commercial projects, this estimate suggests that VIV could be a competitive option in the renewable energy market.

2.3 Past Research

Due to the potential benefits of VIV for energy generation, there has been significant research on utilizing it. Three previous MQPs at WPI have conducted research into VIV in addition to the previously mentioned VIVACE at the University of Michigan.

2.3.1 Past MQPs

There have been three previous WPI MQP projects that experimented on topics of VIV. They focused mainly on different ways to alter the geometry of the converter to maximize the amplitude and frequency of the oscillations. However, none of these projects actually converted VIV into usable power.

In 2011, Hall-Stinson, A. S., et al looked into testing various diameter sizes of the cylinders to locate the correlation between diameter of the cylinder and different variables, including oscillation frequency and mean amplitude. They conducted eighty-five tests with five cylinders of different diameters for various criteria to determine the most ideal cylinder diameter. Several masses were attached to each cylinder and suspended by springs from a fixed point in the channel of their testing tank. The testing tank was an open flow channel with sump pumps integrated to create a uniform and steady flow speed. With their tests, they determined that a cylinder with a diameter of 1” (25.4 mm) produced the best results.

Also in 2011, Distler, D.B., et al experimented with the shape of the cross-sectional body to see what would yield the largest displacement values. Using a typical cylinder as their control group since it is the shape most commonly used in VIV experiments, the group digitally experimented with a variety of additional shapes, such as triangles and ellipses, to determine the optimal shape to build for testing. They concluded that the T-shape produced the largest lift

coefficient so it was chosen, along with a couple T-shaped variations, for their physical testing. Similarly to Hall-Stinson, A. S., et al, Distler, D. B., et al constructed a tank with sump pumps for their experiments. Their results were somewhat inconclusive, however, as they did not determine whether the T-shape was more efficient than the control cylinder.

In 2012, Ball, I.M. et al continued the previous MQP's research by attempting to optimize the shape of the bluff object used. They also determined that the T-shape was the optimal shape and built a tank to test that theory. The bluff objects being tested were attached to a pivoting beam that was designed to have a specified natural frequency. They concluded that the T-shape was the optimal shape and that the lock-in condition resulted in the greatest power output.

2.3.2 VIVACE

As mentioned in Section 2.2.1, the group that has come the farthest in the pursuit of VIV energy is Bernitsas, Raghavan, Ben-Simon and Garcia in their development of the Vortex Induced Vibrations for Aquatic Clean Energy converter (VIVACE) at the University of Michigan.

In their design, a cylinder is held aloft by two springs attached to end plates and constrained so that it can freely vibrate up and down. The apparatus is attached to magnetic sliders that travel along a rail containing a coil. When the system vibrates, the motion of the magnets over the coil generates a DC current that can then be converted to AC and utilized for power (Figure 5).

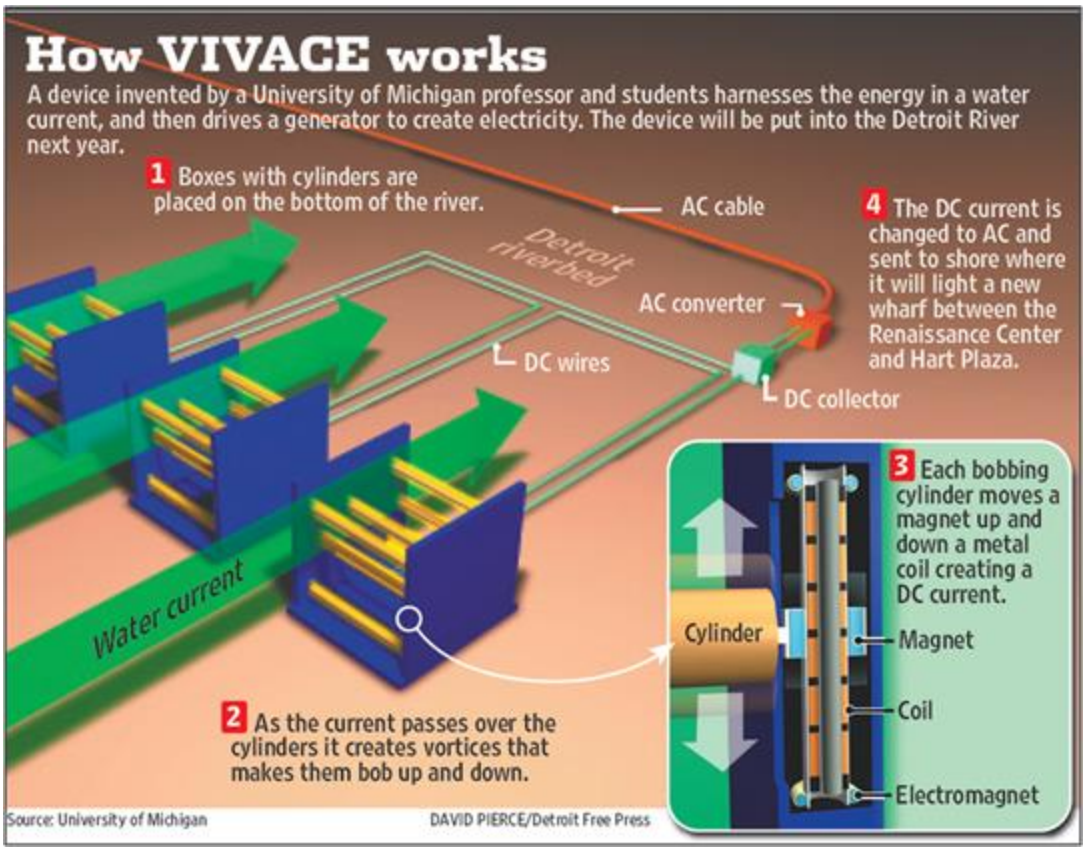

Figure 5: Overview of the VIVACE Converter (Vortex Hydro Energy)

In testing, the system was held stationary in a channel that produced water flow. VIVACE engineers also acknowledged that similar testing results are possible by dragging the apparatus through calm water at a constant velocity. Even at low speeds, VIV can transfer kinetic energy into electricity, unlike more common forms of hydropower such as dams and turbines. This is an advantage because it is a less invasive method of hydropower that can be utilized in locations with less powerful streams. It has a low impact on the environment and can be scaled up or down, depending on the need.

2.3.3 Areas of Interest

The three MQP groups and the VIVACE team have opened up many more avenues of VIV experimentation and research through their studies.

Distler, D.B., et al recommended that the scale of the experimentation be increased. They felt that it would “increase the validity of the data collected and may lead to more conclusive paths to continue work” (Distler, D.B., et al). They also suggested experimenting

with various types of generators to determine the optimal power extraction method.

Hall-Stinson A.S., et al suggested that new tests with a higher fluid velocity/Reynolds number be conducted in order to provide a more realistic condition to test the technology under. They and Ball I. M. also suggested that future groups assess the possibility of conducting tests in large-scale research laboratories such as the Alden Research Laboratory. These large-scale labs have numerous tanks and other equipment designed to test various aspects of hydrokinetic experimentation. Utilizing laboratories of this magnitude would result in cleaner data and less time spent on the construction of a testing tank.

Based on the results and recommendations from the three WPI MQP groups and the team at the University of Michigan, our team concluded that the next step in advancing VIV research would be to construct an oscillator utilizing the findings of the previous MQPs and actually convert the VIV into usable power.

2.4 Energy Harvesting and Measurement

In order to assess the VIV apparatus' ability to harvest energy, it is important to measure the power output of the overall system, potentially using dynamometers or linear force sensors. VIV can also be converted into electrical power utilizing electromagnetic, piezoelectric and electrostatic generators. The following sections will explore each of these options in detail.

2.4.1 Mechanical Energy

One type of energy harvesting is through the production of useful mechanical power that can be used to drive a mechanical process. This often takes the form of a rotating shaft that can be used to drive rotational motion or converted into linear motion. A Dynamometer can be used to measure the rotational mechanical power output. Absorption dynamometers are driven by the motor or power source, and used to measure the power output, usually by measuring the torque and the RPM of the rotating shaft. The load is varied by adding or removing weight to the lever arm (Figure 6) (ME Mechanical).

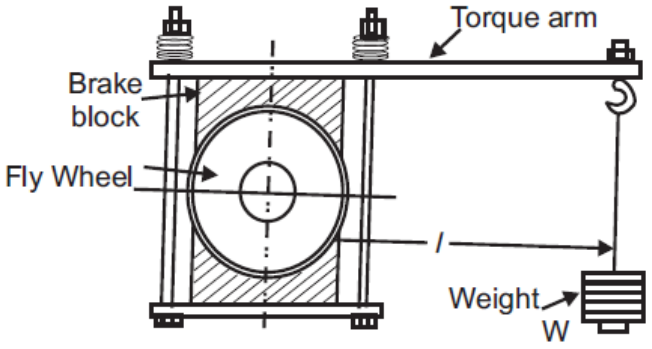

Figure 6: Prony Brake Dynamometer (ME Mechanical)

Dynamometers can be constructed to match the desired scale, making them ideal for applications involving a varying load. However, they have some distinct disadvantages when it comes to VIV applications. First, dynamometers dissipate energy through heat, meaning that they need to be continuously cooled. Second, dynamometers are usually built to measure the power output of a rotating shaft. VIV produces linear oscillatory motion, meaning that the linear motion of the cylinder would have to be converted to rotational motion before the power could be measured or utilized.

Additionally, there are several linear methods of measuring force. These methods include strain gauges, accelerometers, spring-displacement measurement, and linear variable differential transformers (LVDT). These measurements of force can be combined with a velocity measurement to determine the mechanical power.

2.4.2 Electromagnetic Harvesting System

One of the most fundamental methods of electrical power generation uses electromagnetism. Magnetic materials have magnetic moments in them (dipoles) that are randomly organized within the material before it is magnetized. Once an external magnetic field is induced across the material, the dipoles tend to align themselves in the direction of this field. The moments will try to realign themselves along the direction they were previously facing, but they cannot return to the original random orientation. Therefore, the material is considered to be magnetized. These materials are useful in many applications because they can conduct a magnetic field and can be used in the conversion of energy (Umans, S. D.).

Electromagnetic systems generate power by using magnetic fields to convert mechanical energy into electrical energy. When a magnetic material moves through or near a coil it induces

a force on the coil. The resulting force changes the magnetic field, inducing an electromotive force (Equation 15). The amount of electromotive force directly relates to the amount of current that is induced across the circuit through the following equation,

$$Emf = N * i$$

Equation 15

where Emf is the electromagnetic force, *N* is the number of turns of the coil, and *i* is the current induced in the electric circuit. Figure 7 shows the coil *i* wrapped in *N* turns around the magnetic material. The magnetic plunger induces the force that alters the magnetic field within the material. The permeability of the core, μ, determines the reluctances present in the system and can range from that of free air, 4πE-7, to infinity. At infinity, the reluctance of the core is considered negligible. The reluctances of the air gaps are usually considerably larger than those of the magnetic core (Umans, S. D.).

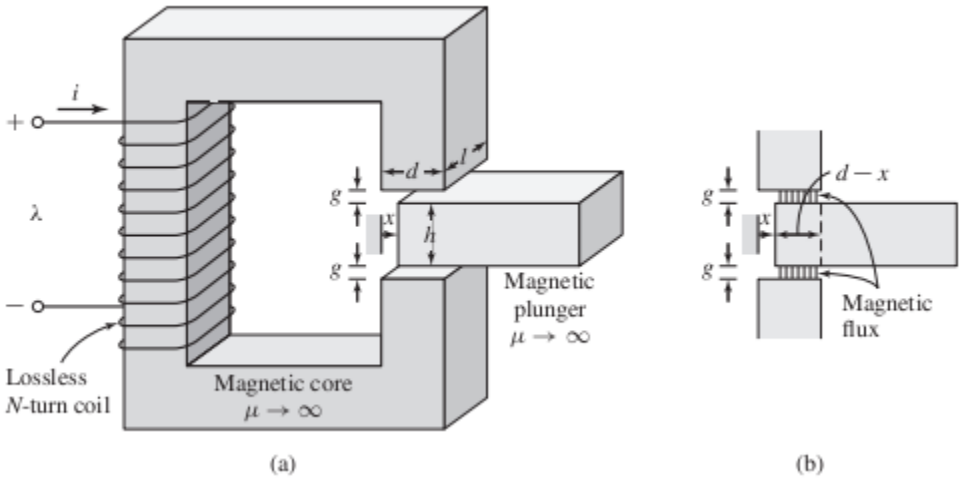

Figure 7: A Theoretical Electromagnetic Set-Up (Umans, S.D.)

Magnetic systems can be modeled as circuits where *N*i* (the electromotive force) represents a voltage, the reluctances of both the core and air gaps can be modeled as resistors, the flux induced in the system is modeled as the current, and the flux density, B, can be modeled as the current density, J. This is significant because the governing equations of normal circuit operations can be applied here in order to perform circuit analysis.

The VIVACE energy harvester employs the use of an electromagnetic linear generator. A senior design project from the University of Michigan worked on assembling the linear generator to fit the VIVACE device in 2008. Figure 8 shows a CAD model of their design

(Avram, P., 2008).

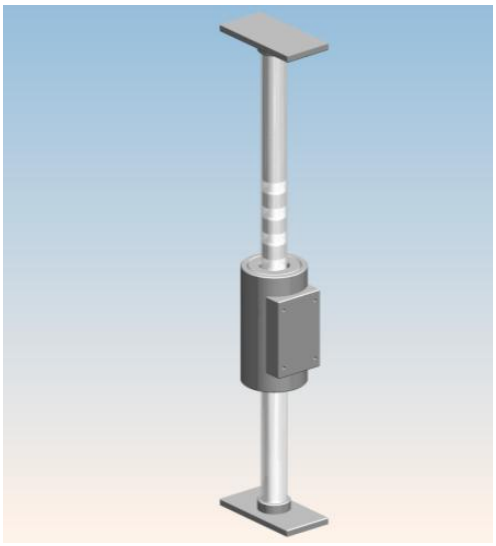

Figure 8: VIVACE Energy Converter Senior Project (Avram, P., 2008)

Their design explored the concept of many different configurations. They ultimately settled on the "alpha design" where Hallbach array magnets and inductors are in series. The use of Hallbach array magnets provides the benefit of having more concentrated flux within the center of the machine. The design uses multiple magnets which allows the device to be scalable and generate greater inductances than a single magnet. However, this also increases the cost of building the linear generator.

2.4.3 Electrostatic

Electrostatic devices use a variable capacitor to generate charges due to motion between two parallel plates. The two parallel plates are separated by air or vacuum, and relative movement between the two plates causes a capacitance variation which generates charge. The electrostatic device is connected to a circuit which can be used to cyclically generate electricity as the capacitor charges and discharges. The energy converted in each cycle can be calculated using the following equation:

$$E = \frac{1}{2} Q^2 \left(\frac{1}{C_{min}} - \frac{1}{C_{max}} \right)$$

Equation 16

Q is the electric charge for a given voltage, C_{min} is the minimum capacitance and C_{max} is the maximum capacitance. The capacitance of the device is determined using a simple plane

capacitance model. Electrostatic devices can be used for vibrational energy harvesting, utilizing the vibration of the cylinder as the two plates move relative to each other (Boisseau, Despesse, & Seddik).

2.4.4 Piezoelectric

Piezoelectric materials have a unique ability to convert mechanical stresses into electrical energy. These materials have crystalline structures and generally contain electric dipoles. When a mechanical stress is applied, it changes the direction of polarization and produces an electrical field (Ledoux, 2011). The amount of voltage that is generated is directly proportional to the stress on the chosen material. Piezoelectricity is useful in small applications because of its small size and broad range of operating frequencies.

Piezoelectricity depends on a combination of the linear electrical behavior of a material (Equation 17) and Hooke's law for linear elastic materials (Equation 18).

$$D = \varepsilon E \qquad \text{Equation 17}$$

$$S = sT \qquad \text{Equation 18}$$

Where D is the electric displacement (C/m^2), ε is the dielectric constant (F/m), E is the electric field strength (N/C), S is strain (m/m), s is the compliance (m^2/N), and T is stress (N/m^2). These equations are combined along with the matrix of the electric permittivity to describe the piezoelectric effect.

Piezoelectric materials are often crystals, such as quartz, and ceramics, such as ZnO, AlN, and lead zirconate titanate (PZT). PZT is the most commonly used piezoelectric material because of its relative cheapness, strength, and durability. Piezoelectric materials often have different properties in different directions. Young's Modulus and compliance do not vary significantly with direction and are generally treated as constants. The piezoelectric charge constant, which is an indicator of the voltage developed due to strain, varies somewhat, but can generally be assumed as constant. The dielectric constant, which is the ratio of the material's permittivity to the permittivity of free space, does vary with direction, but the variance is small compared to the total value. The electromechanical coupling coefficient is an indicator of the material's ability to convert from mechanical to electrical power. The coupling coefficient is generally greater for a rectangular plate displaced lengthwise than for a disk displaced radially. (Piezo Systems). Values often provided by the manufacturer include capacitance, resonant

frequency, maximum voltage, and maximum deflection.

In addition to crystals and ceramics, there are also piezoelectric films, such as polyvinylidene fluoride (PVDF). Piezoelectric films work similarly to ceramic piezoelectrics, except that they are highly flexible. This makes them more suitable for applications with a large displacement. However, one of the limitations of film piezoelectrics is that they are not as effective at electromechanical conversion, particularly at low frequencies. For example, the electromechanical coupling coefficients k_{31} and k_p for PVDF are 0.12 and 0.14, compared to 0.35 and 0.65 for PZT. Copolymers of PVDF have slightly better coupling coefficients of 0.2 and 0.25, but are still not as efficient as ceramics (Measurement Specialties).

Piezoelectric materials are used for power generation by inducing a mechanical stress on a piezo element which is connected to a resistive circuit. The mechanical stress can take the form of bending, compression, or a shear stress (Figure 9).

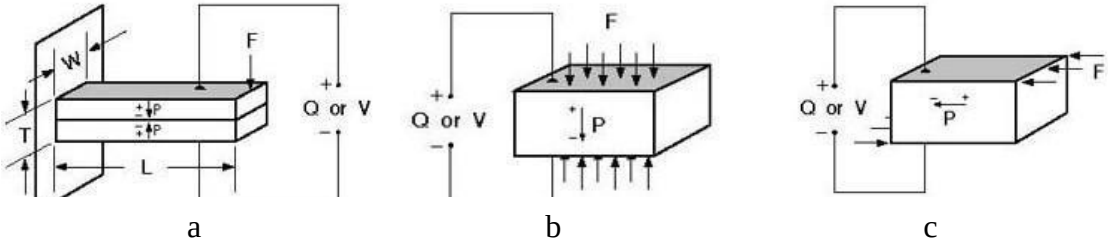

Figure 9: Mechanical Stresses on Piezo Elements: a.) Bending b.) Compression c.) Shear (Piezo Systems)

The mechanical stress on the piezo element generates a voltage differential, which when connected to a resistive circuit, can generate power. For a vibrating or oscillatory system, the piezo element generates an alternating current, so a rectifying circuit is needed to convert to DC. (Figure 10).

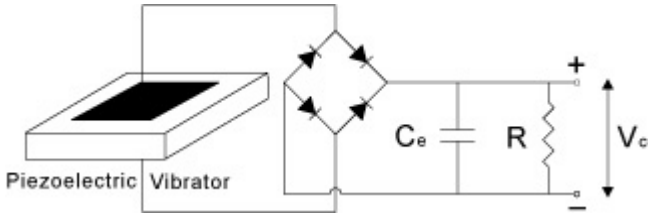

Figure 10: Rectifying Circuit for a Piezoelectric Harvester (Shu & Lier, 2006)

Piezoelectric transducers can be used to harvest frequencies ranging from less than 1 Hz to 1MHz and can have conversion efficiencies of up to 90% However, the actual power and efficiency is generally limited by the vibration amplitude, frequency, force, and size limitations of the harvesting system. For a piezo element acted on by an oscillating force of frequency ω,

the voltage can be determined as follows:

$$V(\omega) = \frac{dF(\omega)\omega Z}{Y}$$

Equation 19

Where d is the piezoelectric charge constant, Y is Young's modulus, and Z is the parallel combination of the capacitance and the load resistance. The power is equal to $V(\omega)^2$ divided by the load resistance. For piezoelectric devices, "the load for maximum power scales inversely with frequency." Therefore the frequency at which the object operates determines the load that the system can handle (Sherrit, S., 2008). The optimal load resistance for power generation in a piezo transducer depends on the equivalent resistance of the mechanical harvesting system it is coupled with. However, the power generation can also be estimated by looking at the optimal load resistance for an uncoupled piezo element. For an uncoupled piezo, the optimum resistance to generate power is defined in Equation 20.

$$R^{\text{opt}} = \frac{\pi}{2C_p w}.$$

Equation 20

R_{opt} is the optimal load resistance in Ohms, C_p is the capacitance of the piezo in Farads, and ω is the frequency the piezo is vibrating at in rad/s (Shu & Lien). Most piezo element manufacturers provide a maximum voltage and an equivalent capacitance for the element. Therefore, the maximum power output of the element can be estimated by dividing the rated voltage of the piezo squared by the estimated optimal load resistance.

2.4.5 Maximum Power Output

A load resistance is required to measure the electrical power output of the system once it has been converted from mechanical to electrical power. When adding a load resistance to the generator and VIV set up, it is important to consider the total Thevenin resistance of the VIV system and generator. This represents the total resistance present in the initial system. In order to achieve maximum power output, the added load resistance must match the internal Thevenin resistance. This will allow for a theoretical efficiency of 50%. There are other instances where the theoretical efficiency can reach greater values, but the power output generated by the machine is reduced. Figure 11 is a graphical representation of the maximum power output compared to the efficiency and demonstrates the key resistance ratio of 1 for maximum power

(Maximum Power Transfer Theorem, 2015).

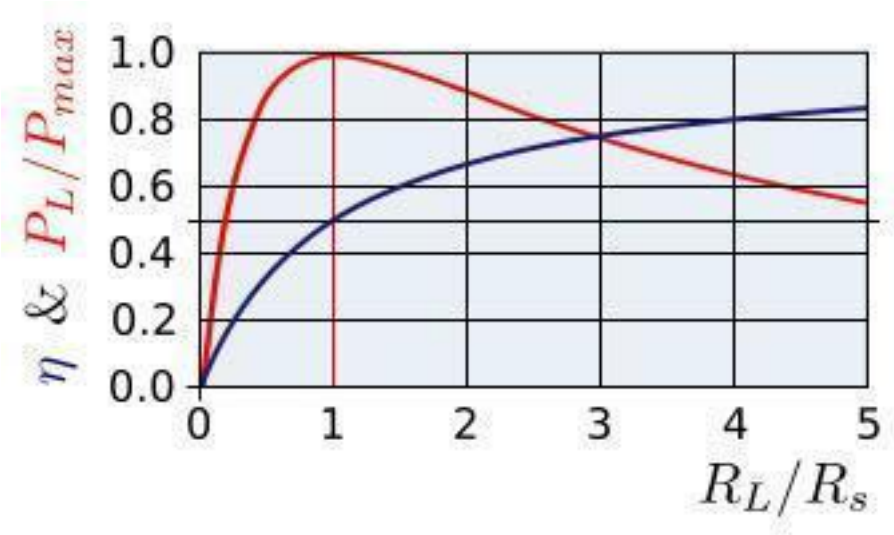

Figure 11: Demonstrates the Maximum Power Output Possible for a Given Resistive Load (Maximum Power Transfer Theorem, 2015)

2.4.6 Selection of Energy Harvesting Method

The energy harvesting system chosen for this project needed to be able to convert the mechanical motion of the vibrating cylinder into usable and measurable mechanical or electrical energy. The mechanical system possibilities considered were dynamometers, accelerometers and pistons, strain gauges and pistons, and linear variable differential transducers (LVDTs) and pistons. The electrical energy conversion possibilities were electromagnetic, piezoelectric, and electrostatic.

Figures 12 and 13 display the decision matrix used to determine a final conversion method. The criteria used to determine the best system were as follows:

- Range: the system is capable of converting displacements of 10-15 mm into usable energy.
- Varying the load: the system is able to vary the load.
- Cost: the system is feasible to purchase with our allotted budget.
- Constructability: the system can be constructed by a team of students who are not experts in the field.
- Ease of measurement: the system produces power that can be easily measured.
- Durability: the system is able to withstand the testing procedures.

	weight								
		dynamometer		accelerometer & piston		strain gauge & piston		LVDT & piston	
Range	10	10	100	10	100	10	100	8	80
Varying the Load	9	8	72	4	36	5	45	3	27
Cost	8	8	64	6	48	9	72	2	16
Constructability	7	5	35	8	56	3	21	8	56
Ease of Measurement	2	6	12	8	16	9	18	7	14
Durability	6	7	42	9	54	7	42	10	60
			325		310		298		253

Figure 12: Mechanical System Decision Matrix

	weight								
		electromagnetic		piezoelectric		electrostatic		Total Potential	
Range	10	5	50	10	100	10	100	10	100
Varying the Load	9	10	90	10	90	10	90	10	90
Cost	8	3	24	10	80	7	56	10	80
Constructability	7	3	21	8	56	2	14	10	70
Ease of Measurement	2	7	14	7	14	7	14	10	20
Durability	6	5	30	5	30	5	30	10	60
			229		370		304		420

Figure 13: Electrical System Decision Matrix

The criteria were then weighted based on how important they were to successfully complete the project. We decided that range was the most important criteria because if the system could not convert energy in the necessary range then measuring the power output would not produce meaningful results. Considering this, we gave the range criteria a value of 10. In contrast, the ease of measurement criteria was the least important at a value of 2 because all of the systems are measurable, though certain systems like the dynamometer might require additional steps and calculations.

We then scored each system on each of the criteria with a number between 0 and 10. A 0 indicates the system did not meet the criteria whatsoever, while a 10 indicates the system excelled in the given criteria. The values were multiplied by their weight value and then added together to identify the system's "score." We then compared each system's score to determine the ideal system. The piezoelectric measurement system had the highest score at 370 out of 420

possible points. The electromagnetic system had the lowest score at 229 points out of the possible 420.

The piezoelectric measurement system was scored the highest because it performed well in the majority of the criteria. It was ranked high for range because there are multiple varieties of piezoelectric materials, which would ensure data measurements in the needed range. It, along with all of the electrical options, scored high for varying the load because this can be done by simply changing the value of a resistor in the circuit. Lastly, piezoelectric material was given 7 out of 10 for ease of measurement because voltage can be easily measured with a multimeter, but the electrical elements need to be waterproof.

3. Piezoelectric Testing and Prototyping

In order to produce power through oscillations, both the VIV oscillator and piezoelectrics need to work independently. The first part of this chapter discusses choosing a piezoelectric material and building a circuit to measure the voltage output of the piezoelectrics. The second part of this chapter reviews the prototype building process and testing of the VIV oscillator.

3.1 Piezoelectric Transducer Testing

There are numerous varieties of piezoelectric materials, ranging in cost and degree of flexibility and sturdiness. In order to test the various kinds of piezoelectric materials and determine the optimal positioning for the material of the system, we tested both ceramic and film piezoelectric materials. The testing procedure for the piezoelectric transducers was an iterative process that evolved as we learned more information. The piezoelectric films were stressed by being pulled taut and inducing oscillating pulses, while the ceramic piezoelectric disks were excited through bending the disks. The baseline testing involved the following procedure:

1. Measure the voltage of each piezoelectric transducer directly with the oscilloscope to see the unrectified voltage peaks.
2. Use the simulation program Multisim to model the rectifier circuit and note the expected output. Include an internal capacitance value for the piezo equal to the value given in the manufacturing specifications to properly model the system.
3. Set the Multisim inputs to 18 Vpk with a frequency of 6 Hz.
4. Use a function generator to ensure that the rectifier circuitry was functioning properly.
5. Set the function generator to 1 Vpk with a frequency of 2 Hz.
6. Plug piezoelectrics into the full bridge rectifying circuit, comprised of four 1N4148 diodes, a resistor that may be varied and a capacitor that may be varied.
7. Compare the results from the Multisim simulation and the actual rectifier circuit output.
8. Test each piezoelectric at resistance values from 5 MΩ to 15 MΩ and capacitor values from 0.1 μF to 10 μF in order to assess the effect on the voltage output.

3.1.1 Measurement Methods

When attempting to measure the voltage peaks present in the circuit, we found that our oscilloscope graphs were incorrect and would clip and offset the waveform. This was due to an unavoidable grounding issue present in the circuit. The rectifier circuit is connected in a way where the negative lead of the input is not connected to ground. The internal grounding of the oscilloscope made it impossible to simultaneously measure both the input and the output waveforms without seeing distortion because the circuit was already grounded. Therefore we elected to measure the input with the oscilloscope and the output with the DMM (Digital Multimeter). A second trial run was done for each test in order to also measure the output waveform with the oscilloscope.

3.1.2 Full Bridge Rectifier

In order to convert the AC output of the piezoelectric devices into a measurable DC value, we employed the use of a rectifier. Figure 14 shows the circuit design used in this project.

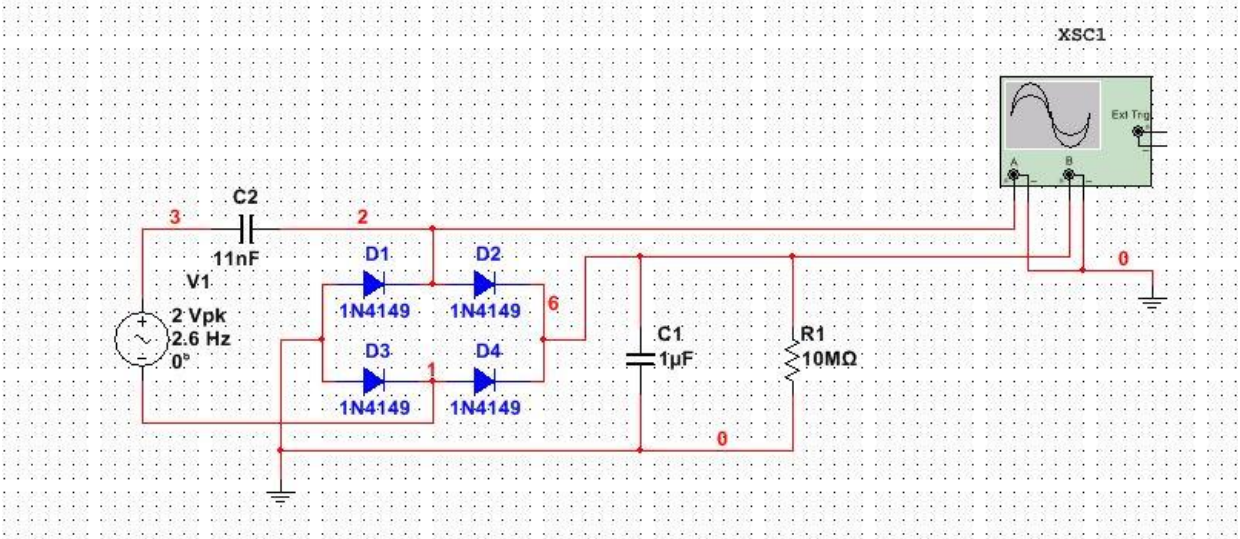

Figure 14: Rectifier Circuit Diagram

The input voltage from the piezoelectric is modeled as a 2 Vpk sine wave at a frequency of 2.6Hz and an internal capacitance of 11nF, which is representative of the larger piezoelectric film. The diodes for the circuit are 1N4184 diodes and it should be noted that the program contained only 1N4149 diodes, but they will function the same as if they were 1N4148 diodes. The load capacitor has a nominal value of 1uF, and the resistance value of 10MΩ. This resistance value will change when determining the optimal load resistance. The XSC1 unit is an

oscilloscope, which is used to display the input and output waveforms. In order to ensure the validity of this circuit design, we simulated it using Multisim, and produced the waveforms shown in Figure 15.

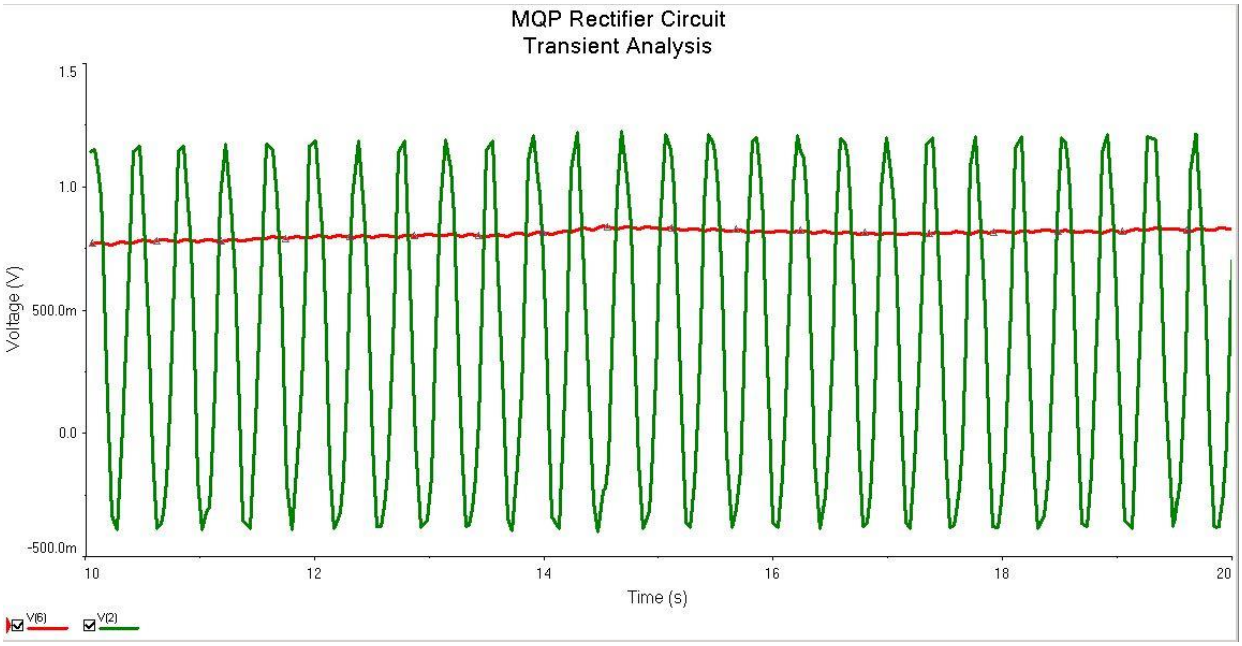

Figure 15: Rectifier Circuit Input and Output Waveforms

The sine wave reflects the AC input, which is distorted due to the presence of the internal capacitance of the piezoelectric. The nearly flat red line represents the output that has been successfully converted to DC. This simulation was performed using a 2 V sine wave, however it can be scaled for larger voltages and the output waveforms would demonstrate this change.

3.1.3 Ceramic Disc Piezoelectric

Ceramic disk piezoelectrics were determined to be inadequate for this experiment. While they were capable of producing 20 V peaks, applying the same magnitude of force as used with the film piezoelectric resulted in cracking. Applying less pressure, in order to avoid cracking, produced consistent peaks at 10 V. Because of their significant fragility, the ceramic material was ruled out as an option.

3.1.4 Film Piezoelectric

Our initial testing revealed that altering the capacitance and resistance in the circuit altered both the output voltage across the resistor and the measured voltage generated from the piezoelectric. The film piezoelectric is modeled as an AC voltage source with a capacitance (Figure 16).

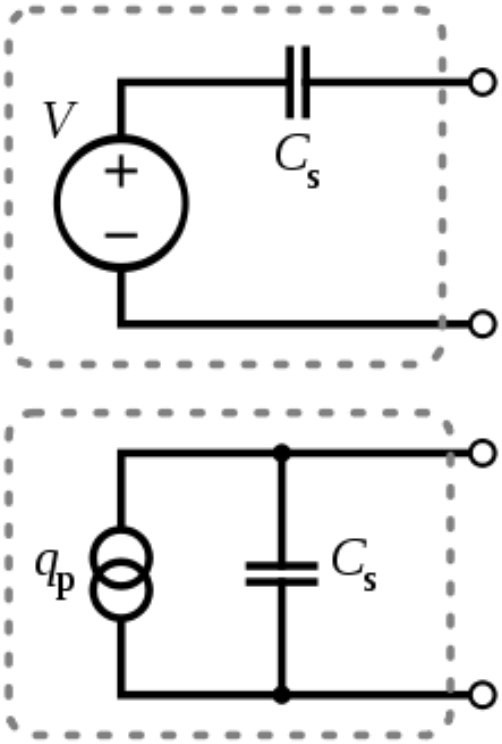

Figure 16: Model of the Film Piezoelectric Voltage Source

The test piezoelectric has an internal capacitance of 2.78 nF and the larger piezoelectric used for prototype testing has an internal capacitance of 11 nF (Measurement Specialties, 2009). We found that a single piezoelectric can produce voltage peaks of up to 50V for either size and that they will produce 100 V spikes when connected in series with a second piezo of the same type and pulled simultaneously.

The piezoelectric is excited by straining the film through applying pressure or stretching. Straining the film under constant tension generated a voltage peak which quickly decayed. This indicates a force must be applied through repetitive pulses in order to continuously generate

electricity. Due to the oscillatory nature of our project, this allowed the piezoelectric to generate continuous electricity as the cylinder vibrated.

3.1.5 Power Output

We measured the voltage output of the piezoelectric used in the prototype when it was not attached to a circuit. The piezoelectric was able to produce voltage peaks of approximately 50 V when sufficiently and consistently pulled taut. Pulling the piezoelectric at a force similar to that expected in the prototype resulted in a voltage that was approximately 10 V. However, this peak voltage is higher than the voltage output when the piezoelectric is connected to the rectifier circuit. The power output can be calculated by dividing the square of the voltage by the measured value of the resistance.

3.1.6 Circuit Components

In our preliminary testing we found that the power output is directly influenced by the values of the resistance and the capacitance. We found that as the capacitance is increased, both the output voltage potential and the voltage ripple are decreased. Voltage ripple is the difference between the maximum and minimum voltages experienced when the capacitor is plugged into the circuit. A lower voltage ripple allows for a more consistent voltage output. A larger output resistance causes a larger voltage output, though it does not necessarily increase the efficiency. Table 1 shows the voltage decrease that occurs as the capacitance is increased by a factor of ten.

Table 1: Voltage Output at Increasing Capacitance

Capacitor (µF)	Resistance (MΩ)	Input (V) (Osc)	Output (V) (Osc)	Output (V) (Dmm)	Comments
0.1	10	8.4	6.2	5.7	Output on Dmm varied by +/-1V, suggests capacitor is too small
1	10	4.8	4.4	4.1	Output on Dmm varied by +/-0.3V
10	10	5.6	5.4	5.0	Took much longer to charge capacitor

The voltage however, increased when the resistance is increased as displayed in Table 2.

Table 2: Voltage Output at Increasing Resistance

Resistance (MΩ)	Capacitance (µF)	Output Voltage (V)	Power Output (µW)
5	1	2	0.8
10	1	3-5	0.9-3.0
15	1	3-5	0.6-2.0

From these resistance and voltage values, we calculated that the overall expected power output is a range between 0.6 and 3 microwatts.

3.2 Oscillator Constraints and Design

The first part of this section outlines the various constraints and dimensions of the testing location. The next part describes the design of the oscillator used as a base for all prototypes.

3.2.1 Testing Location

The testing location was in the WPI rowing tanks, shown in Figure 17. The tanks are able to produce water velocities from 0 to 2 m/s.

Figure 17: Layout of Rowing Tanks

The detailed dimensions of the rowing tank on the left of Figure 17 are shown in Table 3. These dimensions were taken from a previous MQP that used the rowing tanks for prototype

testing (Costanzo, 2015).

Table 3: Rowing Tank Dimensions

Total Length (L)	47’ (14.3m)
Water depth at L = 0m	14.75” (0.37m)
Water depth at L = 7.62m	13.00” (0.33m)
Water depth at L = 14.33m	11.00” (0.28m)
Width of flat bottom	44” (1.12m)
Width of tank (including ledge)	100” (2.54m)
Height of narrow ledge from bottom at 0m	25” (0.635m)

The water depth of the rowing tank is not constant. Table 3 shows that the water is deepest at L = 0m, or the side of the tank closest to the drain. In order to maximize the amount of underwater space for our prototype, we conducted testing on this side of the tank. The water depth at this location is 0.37m, which limited the height of the VIV harvester.

Use of the rowing tanks required our design to have special considerations to prevent any damage to the rowing tank during testing. Because of this, we suspended our prototype in the water from above so that it did not come into contact with the tank lining. Figure 18 shows the height of the tank ledge from the bottom is 25” (64cm).

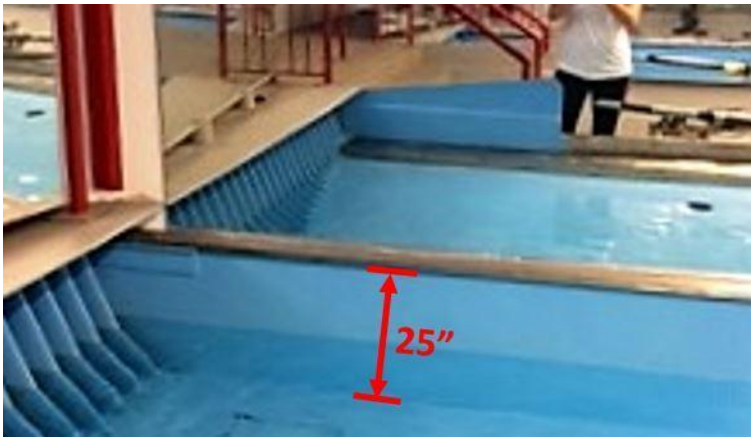

Figure 18: Rowing Tank Bottom-to-ledge Height

Another crucial dimension is the distance across the tank from ledge to ledge, shown in Figure 19. Including both ledges, the previous MQP group measured the distance to be 100” (2.54m).

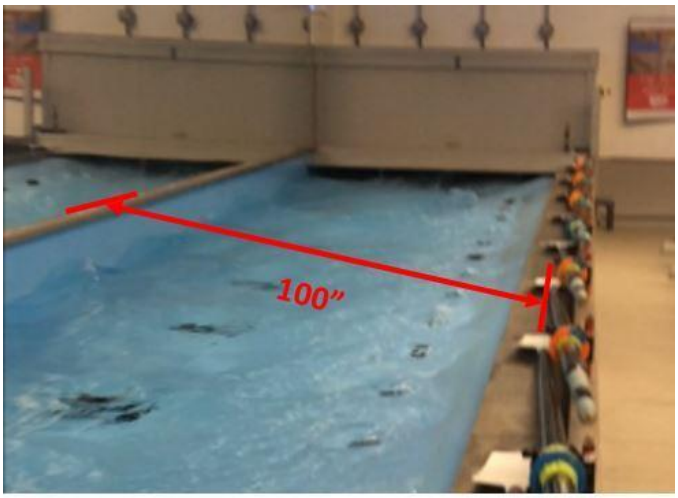

Figure 19: Rowing Tank Width

The last critical dimension of the rowing tank is the flow speed. The tank flow is controlled by a panel that has speeds in arbitrary units ranging from 0 to 2000. A flow tank speed of 100 units is approximately equal to 0.1 m/s, so the tanks can produce flow ranging from 0 to 2 m/s. The open channel flow in the tank is turbulent, because it has a theoretical Reynold’s number of 5.24E5 at a speed of 0.5 m/s, which replicates real world conditions.

3.2.2 Oscillator Design

The general design of the oscillator was determined from our testing location, the piezoelectric energy harvesting system, and our VIV calculations. It consists of a tank rig, VIV oscillator, and frame.

The tank rig is the simplest design component. To prevent damage to the rowing tanks, the prototype was suspended from two 2x4 beams spanning the width of the tank. Two additional 2x4s were attached across the beams in order to improve stability. The brackets used to attach the frame to the beams were 6” zinc-plated corner braces. The holes for the corner braces were drilled 38cm and 71cm from the far end of the beams to ensure that the prototype was positioned over the flat bottom of the tank. The tank rig assembly is shown in Figure 20.

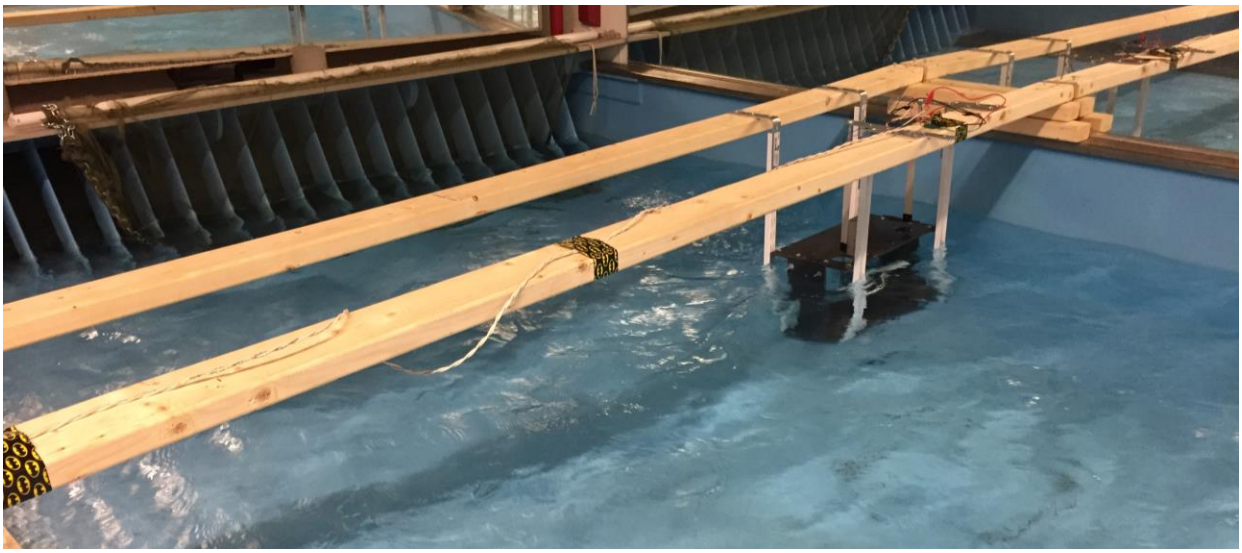

Figure 20: Tank Rig Set Up

The VIV oscillator consisted of a cylinder attached in parallel to four springs. The dimensions of the cylinder were determined using the linear harmonic oscillator model described in Section 2.1.5. Some important parameters and calculations from this model are shown in Table 4.

Table 4: Parameters Used for Amplitude and Power Estimation

Cylinder Length (L)	0.229 m	**Reynolds Number**	1.346E4
Flow Speed (U)	0.5 m/s	**Strouhal Number**	0.2
Cylinder Diameter (D)	0.0269 m	**Coefficient of Lift (C_L)**	0.5
Vortex Shedding Frequency (ω_s)	23.3 rad/s	**Natural Frequency (ω_n)**	25.3 rad/s
Spring Constant (k)	182 N/m	**Damping Ratio (ζ)**	0.10
Mass of Pipe	0.127 kg	**Added Mass**	0.130 kg
Density of Water (ρ)	998 kg/m^3	**Reduced Velocity (U*)**	4.41

The coefficient of lift was assumed to be 0.5 and the damping ratio was assumed to be 0.1. These assumptions were based on measured coefficients of lift and damping ratios from previously conducted experiments at similar Reynold's numbers (Williamson & Govordhan, 2008). The calculated Reynolds number is within the range of 300 to 10^5 that VIV occurs. The cylinder chosen based on these calculations was a ¾" nominal diameter, 9" (23cm) long PVC pipe fitted with PVC end caps.

Given these values, the following equations were used to calculate the maximum amplitude, lift force, and power output:

$$A = \frac{\rho U^2 D L C_L}{2k * \sqrt{[1 - (\omega_s/\omega_n)^2]^2 + (2\zeta\omega_s/\omega_n)^2)}}$$

$$F_L = \frac{1}{2}\rho U^2 D L C_L$$

$$P_{max} = \frac{\omega_s \rho^2 U^4 D^2 L^2 C_L^2}{4k * \sqrt{[1 - (\omega_s/\omega_n)^2]^2 + (2\zeta\omega_s/\omega_n)^2)}}$$

Equation 21

From these equations, the maximum amplitude was calculated to be 7.4cm, the maximum lift force was 0.38 N, and the maximum theoretical mechanical system power was 0.066 W.

The oscillator design used four springs connected in parallel to suspend the cylinder. The desired spring constant for each spring was a quarter of the total spring constant of 182 N/m (Table 4). Therefore we chose each spring to have a value of 45.5 N/m. In order to handle a maximum displacement of 7.4cm in either direction, the springs each needed to be able to extend approximately 15cm from the starting position. Extension springs were found from McMaster Carr with a stiffness of 42 N/m, an extended length of 18.6cm.

The final component of the design was the frame, which houses the oscillator and connects to the tank rig. A model of the entire frame and tank rig assembly is shown in Figure 21.

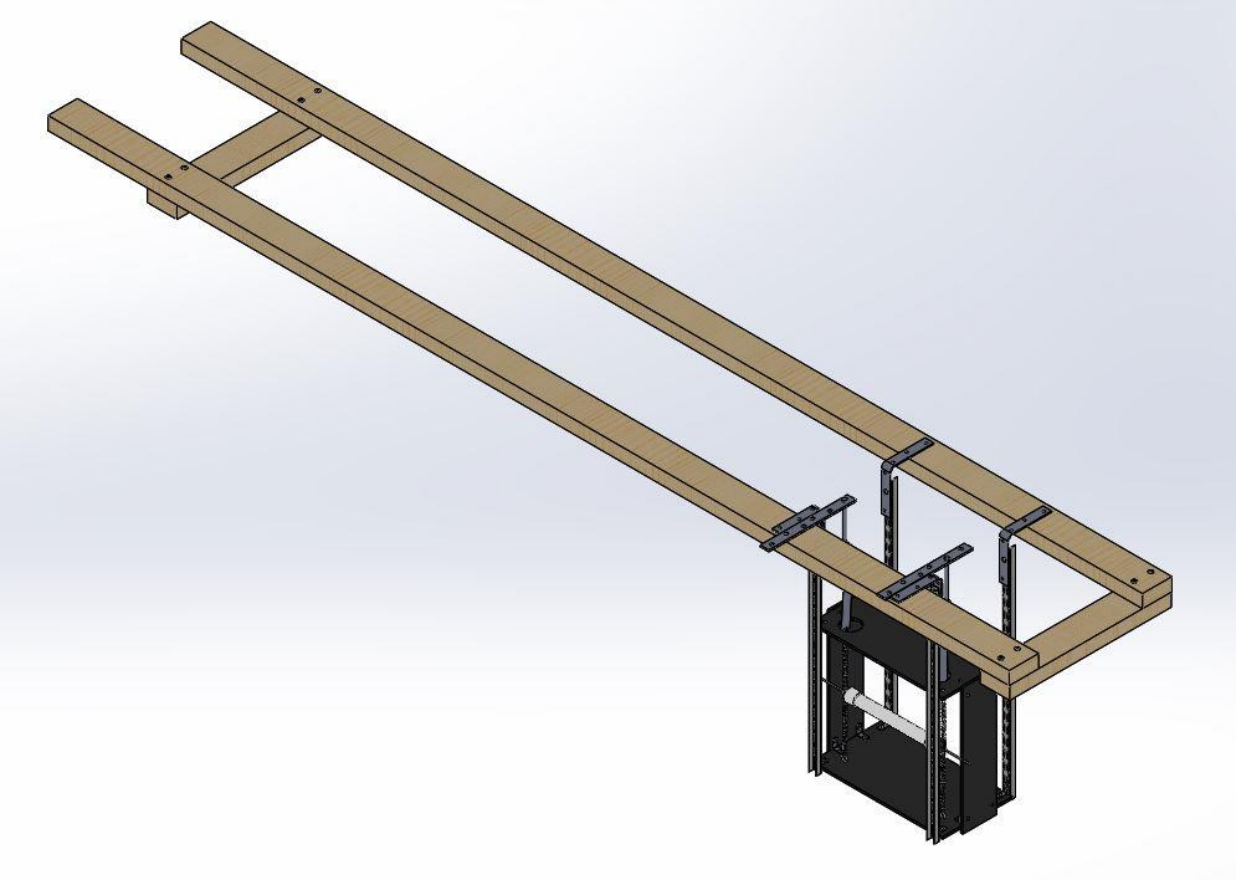

Figure 21: Oscillator Frame and Tank Rig

The four vertical struts of the frame were 25” shelving brackets. The bottom and top shelves, and the side panels, were cut from ¼” PVC sheets. The PVC sheets were attached to the shelving brackets using 1” zinc-plated corner braces. The holes at the top of the shelving brackets were fastened to the larger corner braces of the tank rig which allowed the tank rig to be detached from the frame.

In order for the frame to house the springs and allow them to fully compress and extend as needed, the height of the frame from the base to the top plate needed to be at least the combined length of the springs at full extension. This height also allowed for a 5cm clearance between the bottom of the frame and the bottom of the tank. The width of the frame is based on the length of the cylinder. To allow the springs to attach and the cylinder to connect to sliders or slots to constrain lateral motion, a 5cm clearance was given on each side, for a total width of 38cm. A dimensioned drawing of the frame is shown in Figure 22.

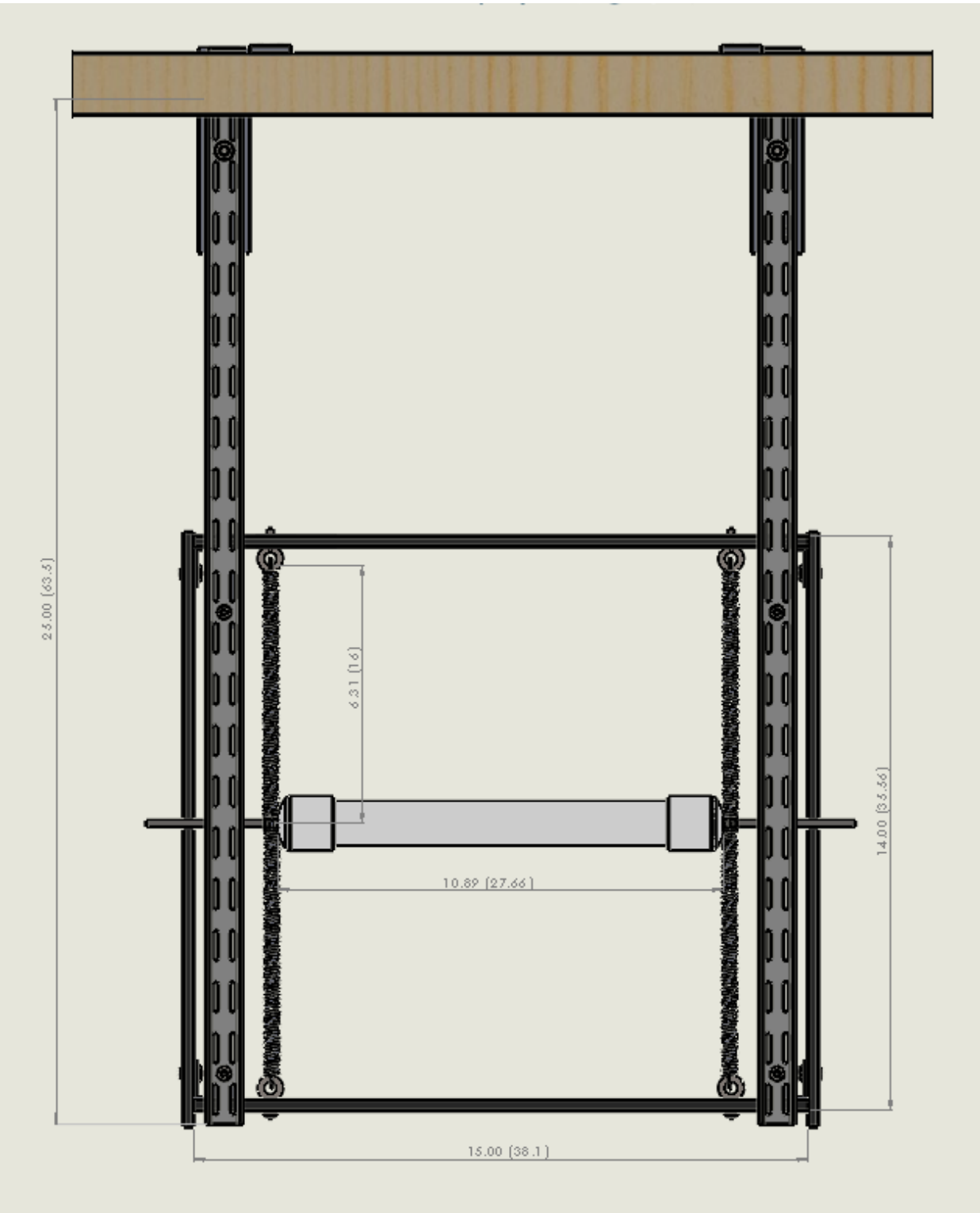

Figure 22: Oscillator Frame

Holes were drilled in the PVC end caps so screws could be placed extending out from either end of the cylinder. The springs were secured to the screws using nuts. The screws were

also used to connect to various sliding and slot mechanisms used to constrain the cylinder motion. These mechanisms are discussed in Section 3.4.

In order to measure the displacement of the cylinder visually, we attached a ruler to the far side of the frame. A red wire that extended above the water level was attached to one of the cylinder screws. When viewed from the side of the rowing tank, the wire was seen moving in relation to the ruler and the displacement was measured.

3.3 Testing Procedures for Oscillator Prototypes

3.3.1 Flowing Water Tests

Each prototype was tested in flowing water in the rowing tanks to see if VIV occurred. If oscillation was observed, the amplitude and frequency of the oscillations were measured using a ruler, high speed camera, and Logger Pro's video analysis tool. Each prototype was tested using the following procedure:

1. Attach the ruler to the side of the oscillator.
2. Attach the pole with the netting to the end of the tank and lower the net so that it covers the entrance to the drain.
3. Attach the oscillator to the wood frame and suspend the assembly in the water.
4. Set up the high speed camera on a tripod and position it so that the red wire attached to the cylinder and the ruler are clearly visible and in focus.
5. Turn the rowing tanks to the lowest speed setting, which is about 100. Wait until the water is flowing in the correct direction. This can take several minutes as the rowing tank builds up speed.
6. Increase the speed of the flow by increments of 50. At each interval wait at least two minutes for the flow to reach a constant speed.
7. If oscillation is observed record a video, clearly stating what speed the tank is set at. Record at least 3 videos at each speed. Once any oscillation has been observed, record videos of every subsequent speed.
8. Continue this process up to a tank setting of 800 or until the cylinder ceases to vibrate.
9. Once all the videos have been taken, turn the speed of the rowing tanks down to zero and ensure that the screen has gone blank and the tanks are turned off.

10. Remove the entire apparatus from the water and detach the oscillator prototype from the wood frame.
11. Import each video into Logger Pro and use the video analysis tool to plot the motion of the red wire in the vertical direction. Use the ruler to set the scale on the video and the tip of the red wire as the reference point.
12. Perform a sine function curve fit on the graph to obtain the frequency and average amplitude of the oscillations.
13. Record the maximum and minimum displacement.

3.3.2 Still Water Tests

The damping coefficient and damped natural frequency of each oscillator prototype was tested by measuring the oscillations of the cylinder in still water using the following procedure:

1. Attach the ruler to the side of the oscillator.
2. Submerge the oscillator in water.
3. Set up the high speed camera on a tripod and position it so that the red wire attached to the cylinder and the ruler are clearly visible and in focus.
4. Start recording a video on the camera. Push the cylinder down approximately two inches and release.
5. Wait for the oscillations to stop, and then push the cylinder up approximately two inches and release.
6. Repeat steps 5 and 6 at least 5 times.
7. Stop recording, remove the entire apparatus from the water, and detach the oscillator prototype from the wood frame.
8. Import the video into Logger Pro and use the video analysis tool to plot the motion of the red wire in the vertical direction. Use the ruler to set the scale on the video and the tip of the red wire as the reference point.
9. Perform a damped harmonic oscillator curve fit on the y-direction displacement graph to obtain the damped natural frequency.
10. Measure the amplitude of two successive peaks on the graph and use the logarithmic decrement method from Equation 6 to calculate the damping coefficient of the system. If possible, repeat this process for each set of peaks of the oscillation before it converges to zero.

11. Calculate the undamped natural frequency of the system using the measured damped natural frequency and the damping coefficient.
12. Calculate both the total mass of the system using the natural frequency and total spring stiffness and the mass ratio using Equations 3 and 4.

3.4 Oscillator Prototypes

The original frame and testing rig design, including the cylinder dimensions, remained unchanged during prototype testing. However, the method of constraining the cylinder movement was varied in order to achieve oscillation. These changes are detailed in the following sections.

3.4.1 Prototype #1: Drawer Sliders Design

3.4.1.1 Design

The sliders used in this prototype are 22” Liberty Full Extension Ball Bearing Side Mount Drawer Slides, shown in Figure 23. Holes in the base of the sliders were utilized to attach to the PVC side panels. Slots were cut in the top PVC shelf to accommodate the top of the sliders, which protrude above the shelf. The moving component of the slider was cut down to its minimum possible length of 10” in order to reduce the mass of the cylinder assembly. Holes in this moving slider were used to mount the screws that connect to the cylinder end caps.

Figure 23: Drawer Sliders

3.4.1.2 Results

The original drawer slider design was tested twice. In the first test, the flowing water testing procedure outlined in Section 3.3.1 was conducted, but VIV did not occur in the system.

The still water testing procedure outlined in Section 3.3.2 was then conducted to measure and calculate the average damping, the damped natural frequency, the total mass and the mass ratio. The results of the first test are shown in Table 5.

Table 5: Still Water Testing Results for Prototype #1

Total Spring Constant (N/m)	Damping	Damped Natural Frequency (rad/s)	Damped Natural Frequency (Hz)	Total Mass (including added mass) (kg)	Mass Ratio
133	0.258	17.0	2.71	0.444	3.42
357	0.245	26.9	4.77	0.462	3.67

Our measured damped natural frequency of 17.0 rad/s was lower than the target vortex shedding frequency of 23.3 rad/s. For vibration to occur these frequencies need to be approximately equal. To increase the natural frequency of the system we decided to increase the spring constant.

The drawer slider design was modified to have a total spring constant of 357 N/m and the tests were repeated. VIV did not occur in the system and the results from both the flowing water and still water testing procedures are shown in Table 5.

The cylinder did not vibrate even with the increased natural frequency. We concluded that the mass ratio of the system was too large since the lock-in range for large amplitude oscillations disappears for mass ratios greater than 3.4 (Modir, 2016).

The mass included was the cylinder, end caps, screws and associated hardware, and the moving piece of the drawer sliders. We concluded that the drawer sliders were contributing the most to the mass. As a result, we replaced the heavy drawer sliders with a lighter slider option for the second prototype.

3.4.2 Prototype #2: Sleeve-bearing Guide Rail Design

3.4.2.1 Design

The new sliders in prototype #2 consisted of a 1.7cm wide low-profile sleeve-bearing guide rail and its corresponding carriage, shown in Figures 24 and 25.

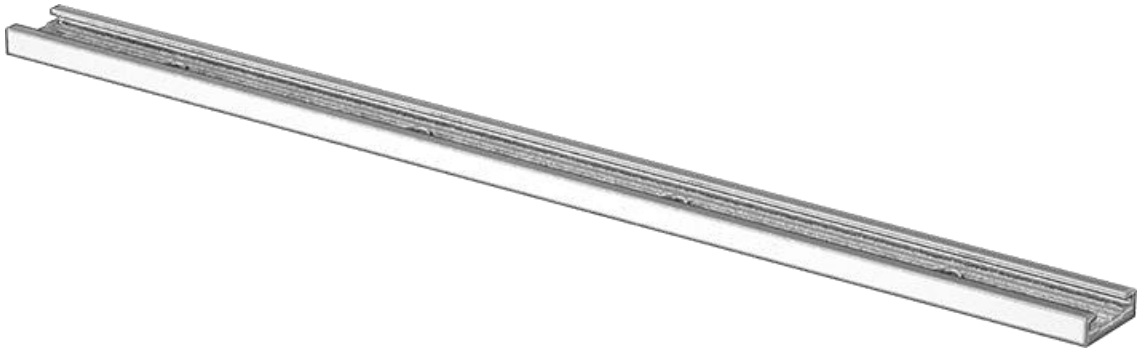

Figure 24: Sleeve-bearing guide rail from McMaster-Carr

Figure 25: Sleeve-bearing carriage from McMaster-Carr

As in the previous prototype, the side panels were used to mount the guide rails. The screws in the cylinder end caps were changed to M3 screws in order to fit the threaded holes in the carriages. Instead of a single screw on each side of the cylinder as in prototype 1, two screws were mounted in the cylinder end caps in order to balance the forces on the carriage when the cylinder moves.

3.4.2.2 Results

Prototype #2 was not tested in the rowing tank because the sliders were unable to move vertically without one side becoming stuck. The narrow tolerance of the carriage and rail caused the carriage to stick when it did not move exactly parallel to the rail. Since the cylinder could not remain perfectly horizontal when oscillating, the carriages could not be kept parallel and the sliders were unusable.

3.4.3 Prototype #3: Freely Suspended Cylinder Design

3.4.3.1 Design

In the third prototype, sliders were abandoned altogether due to the frictional and mass issues experienced in previous prototypes. The cylinder was allowed to move freely in any direction, constrained only by the extension of the springs.

3.4.3.2 Results

Prototype #3 successfully oscillated during the flowing water testing procedure. Movement was first observed at a water speed setting of approximately 400 (0.44 m/s), with maximum oscillations at 600 (0.70 m/s). The analysis from Logger Pro returned the data shown in Table 6.

Table 6: Flowing Water Results for Prototype #3

Water Speed Setting	Average Amplitude (mm)	Maximum Total Displacement (mm)	Average Frequency (rad/s)	Average Frequency (Hz)
605	16.1	42.9	16.8	2.67

Figure 26 shows a graph of the vertical displacement of the cylinder during the flowing water tests at a speed setting of 605 (0.71 m/s).

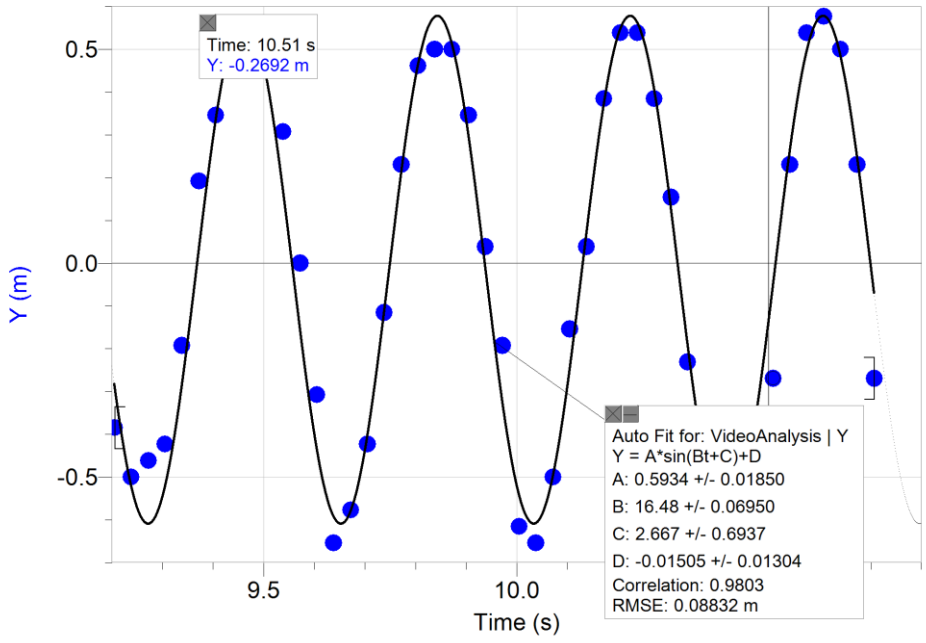

Figure 26: Oscillation Height vs. Time, Rowing Tank, 605 speed

The still water test was performed to get the damping, natural frequency, and mass values for the freely suspended system. The results of the still water test are shown in Table 7.

Table 7: Still Water Testing Results for Prototype 3

Total Spring Constant (N/m)	Damping	Damped Natural Frequency (rad/s)	Damped Natural Frequency (Hz)	Total Mass (including added mass) (kg)	Mass Ratio
133	0.0268	23.7	3.77	0.242	1.86

Figure 27 shows a graph of the cylinder vertical displacement from the still water test.

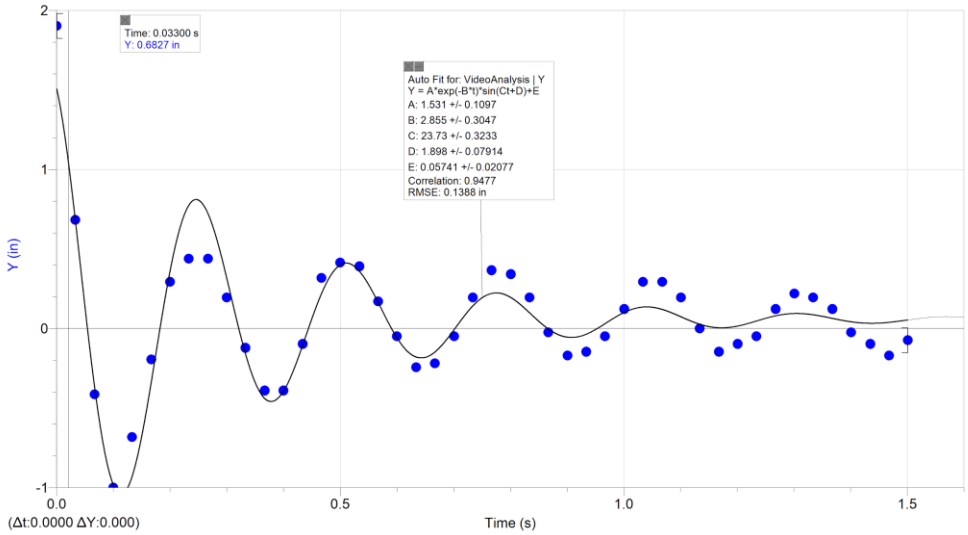

Figure 27: Oscillation Height vs. Time, Still Water Test

The testing of this design was conducted mainly to determine whether or not VIV could be achieved in a free system, i.e. without the sliders or restrictions in the x-direction. While VIV successfully occurred with oscillations between 2.5cm and 4.3cm, the system encountered many issues. For one, the cylinder would sporadically become stuck above 0.70 m/s because of the force of the water flow pushing it against the side panels of the frame. The oscillation frequency was lower than expected at an approximate speed of 17 rad/s as opposed to 23 rad/s. This test confirmed that it was necessary to create a design with a way to constrain the horizontal movement of the cylinder.

3.4.4 Prototype #4: Slot Design

3.4.4.1 Design

In order to constrain the lateral motion of the cylinder and avoid the mass and friction problems of the two slider designs, the final prototype featured a slot design. The side panels previously used to mount the sliders and rails were repurposed and aligned to create a vertical edge. The spring hooks were moved from the middle of the shelves to 5cm from the front edge in order to orient the cylinder in front of the newly-created vertical edge. Since the flow of the water pushes the cylinder against this edge, it was concluded that a vertical edge upstream of the cylinder was not necessary. Since the slot cannot completely constrain lateral motion like the sliders, the bolts on either side of cylinder were extended to ensure the cylinder would not derail during testing. Additionally, the total spring constant was increased from 133 N/m to 182 N/m to account for the additional mass of the screws and nuts attached to cylinder. The final prototype is shown in Figure 28.

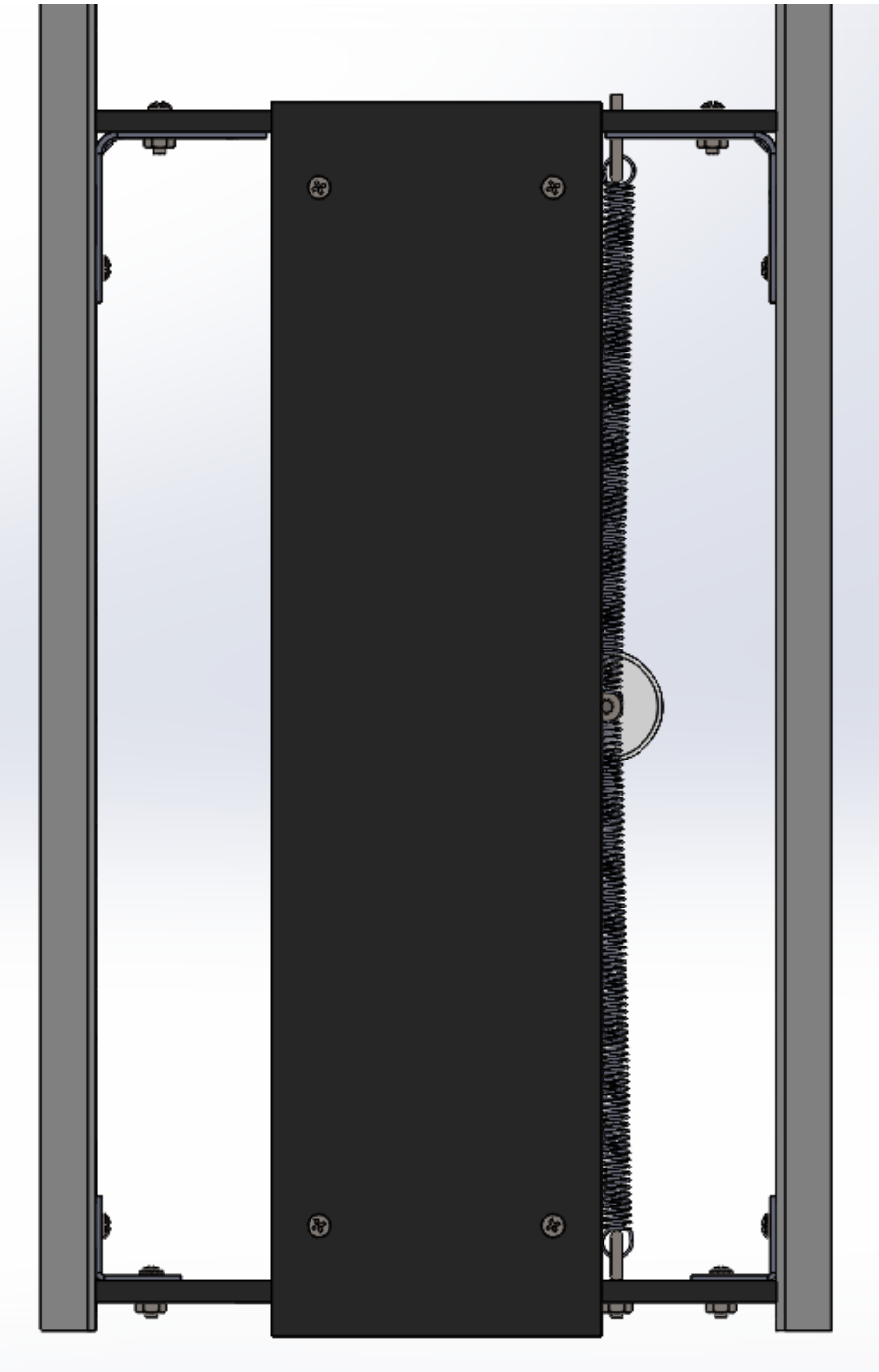

Figure 28: Slot Design

3.5.4.2 Results

In the initial testing of the slot prototype, VIV occurred successfully during the flowing water tests. As shown in Table 8, the amplitude and oscillation frequency increased with flow speed. A still water test to determine the damping of the system could not be performed for this

design because the damping increased with flow speed as the screws were pushed against the plastic edges. For calculations a damping value of 0.1 was assumed.

Table 8: Flowing Water Results for Slot Design Prototype

Flow Speed Setting	Water Velocity (m/s)	Average Amplitude (mm)	Maximum Total Displacement (mm)	Oscillation Frequency (rad/s)	Oscillation Frequency (Hz)
500	0.57	5.4	16.5	17.5	2.78
550	0.64	8.2	22.7	18.3	2.91
600	0.70	11.8	29.8	19.9	3.17

Table 9 shows how the measured amplitude and frequency compared to the values predicted using the linear harmonic oscillator model. The measured results closely matched the predicted behavior, but had a consistently lower amplitude and frequency than predicted.

Table 9: Predicted and Measured Amplitude and Frequency

	Amplitude (mm)		Frequency (Hz)	
Water Velocity (m/s)	**Predicted**	**Measured**	**Predicted**	**Measured**
0.57	7.4	5.4	3.71	2.78
0.64	9.2	8.2	4.83	2.91

Although this prototype successfully vibrated, the oscillations would stop and start sporadically. This problem became worse as the flow speed increased. The mass and positioning of the oscillator were varied to try to improve the consistency of the oscillations, but the breaks in oscillation were not completely resolved. One explanation considered for this was that the inconsistent flow speed of the rowing tanks could be interfering with VIV of the

cylinder. The team therefore decided to obtain a water velocity probe in order to be able to measure the water velocity over time.

4. Methodology

The goal of this project was to utilize piezoelectric transducers to transform the VIV oscillations of a cylinder to electrical power. We achieved this goal by following these objectives:

1. Construct piezoelectric oscillator system using conclusions from preliminary testing.
2. Conduct flowing water testing to determine the water's velocity.
3. Determine the optimal load resistance of the VIV system.

4.1 Energy Harvester Design

The final energy harvester design consisted of two piezoelectric transducers attached to the final oscillator prototype. Two 10" flat mending plates were attached to the wooden beams of the frame so that they extended over oscillator. Five inch screws were connected to the mending plates. Each piezoelectric transducer was epoxied to a 2" corner brace, which was attached to the screws using two nuts. The top of each piezo was also coated in silicone gel to waterproof the electrical leads.

Large holes were cut in the top plate of the oscillator so that the top set of springs could extend through the plate unobstructed. The bottom of each piezoelectric was then epoxied to the top of the springs. In this setup the piezoelectrics act as two additional springs in series with the top set of springs and help to suspend the cylinder, as seen in Figure 29. The piezoelectrics each had an effective spring constant of 66 MN/m. When connected in series with the top springs the total spring constant for the system was 182 N/m, which was exactly the same as the total spring constant for the oscillating system with no piezoelectrics attached. Several iterations of the harvester design were tried with the piezoelectrics attached in parallel to the springs. The cylinder did not vibrate with the parallel setup because the system spring constant was increased to 131.8 MN/m. This spring constant would require a flow speed of 481 m/s, which is well beyond any reasonable flow.

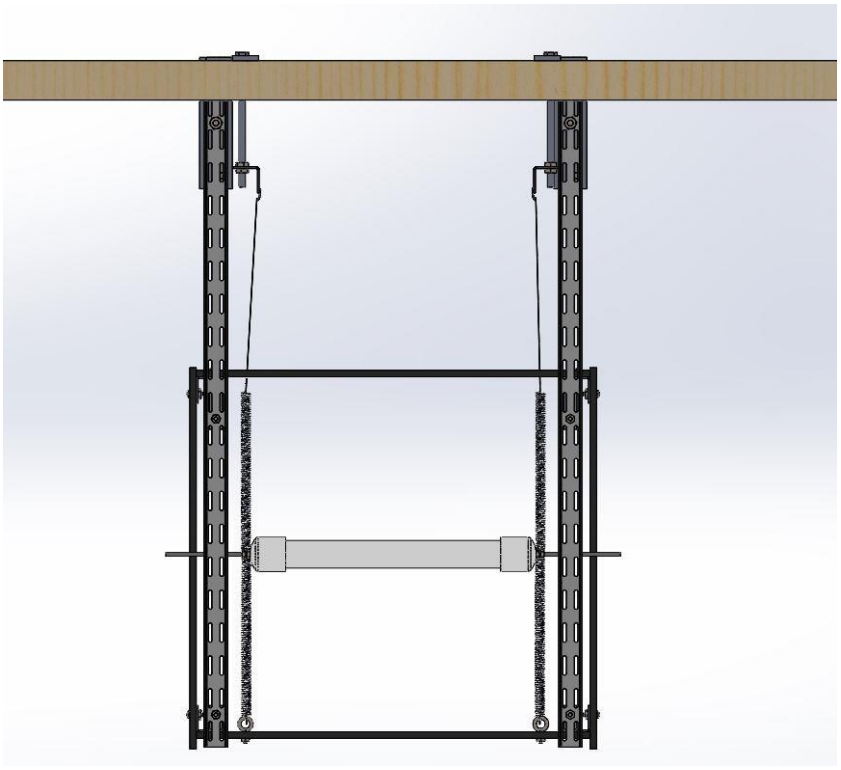

Figure 29: Connection of Piezoelectrics to the Oscillator

The piezoelectrics electrical leads were connected in series using alligator clips, and they were attached to the rectifying circuit using two wires that ran the length of the wooden frame. The rectifying circuit was kept in a waterproof container and attached to the wooden frame outside of the tanks using velcro. Two wires extended outside of the container that were connected to a multimeter in order to measure the output voltage.

4.2 Flowing Water Testing Procedure

The flow speed of the rowing tanks was measured using a Vernier velocity sensor. The velocity sensor was attached using a pipe bracket and was positioned so that the sensor was 18cm from the bottom of the tank and 98cm from the mirrored wall. The velocity sensor was used to measure the water velocity of the tanks at flow speeds of 200, 300, 400, 500, 550, 600, and 650. The initial water level of the tanks was measured using a measuring tape. The tank speed was then increased incrementally and the water velocity was recorded for two minutes at each speed. Because the oscillator worked the best at a tank speed setting of 600, the team recorded 10 minutes of velocity data at this setting. The testing setup is shown in Figure 30.

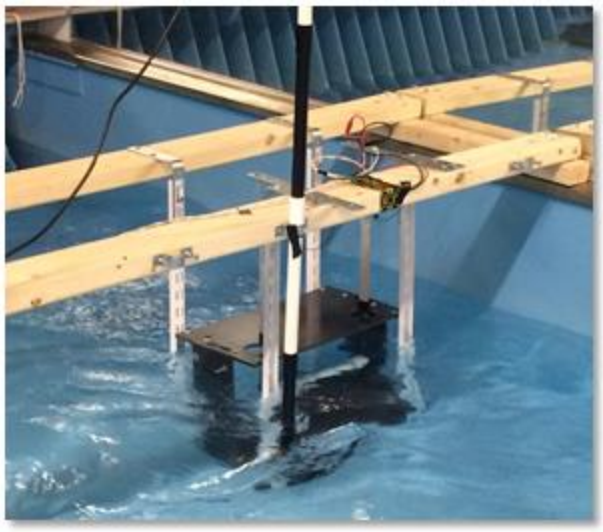

Figure 30: Energy Harvester Testing Setup

The power output of the final energy harvester was measured using a handheld digital multimeter. The procedure for measuring the power output is as follows:

1. Attach the oscillator, including the piezoelectrics, and the Vernier velocity probe to the wooden frame.
2. Connect the piezoelectric leads in series to the rectifying circuit.
3. Connect the velocity sensor to a Vernier LabPro, connect the LabPro to a computer, and open LoggerPro on the computer. Change the sample rate for the flow sensor to 1 sample/second.
4. Place the assembly in the rowing tanks.
5. Connect the rectifying circuit output to the multimeter.
6. Increase the flow speed of the tanks until oscillation is observed. Record the water velocity from the sensor and use a camera to record the output voltage during the oscillation. Also record the flow speed setting of the rowing tanks.
7. Stop the flow and remove the test rig from the rowing tanks.

4.3 Optimal Load Testing Procedure

Although the cylinder vibrated during the flowing water tests, it was not able to sustain oscillations for more than 3 minutes. Because of the short duration of the oscillations it was not possible to vary the electrical load of the system during the flowing water tests. Therefore, to find the optimal load resistance for the system the harvester was tested outside of the water. The

piezoelectrics were connected to the rectifying circuit and the cylinder was oscillated by hand to a displacement of 0.5” (1.3cm) at an approximate frequency of 2.6 Hz. A ruler was used to ensure the correct displacement and a metronome was used to move the cylinder at the desired frequency. The output of the rectifying circuit was connected to an oscilloscope which was used to measure the output voltage. The load resistance was varied from 511 kΩ to 32 MΩ and the voltage was recorded. The power output for each resistance was calculated using $P = \frac{V^2}{R}$, where V is the voltage and R is the resistance.

5. Results

In this chapter we discuss the results of the energy harvester design from flowing water and optimal load testing. We also examine the water flow of the rowing tanks.

5.1 Rowing Tank Water Velocity

The water velocity of the rowing tanks was tested independently to examine flow speed variation and obtain accurate water velocity measurements for each tank setting. The water velocity was measured with a Vernier velocity probe and plotted with Logger Pro. Figure 31 below shows the actual water velocity for various tank control settings.

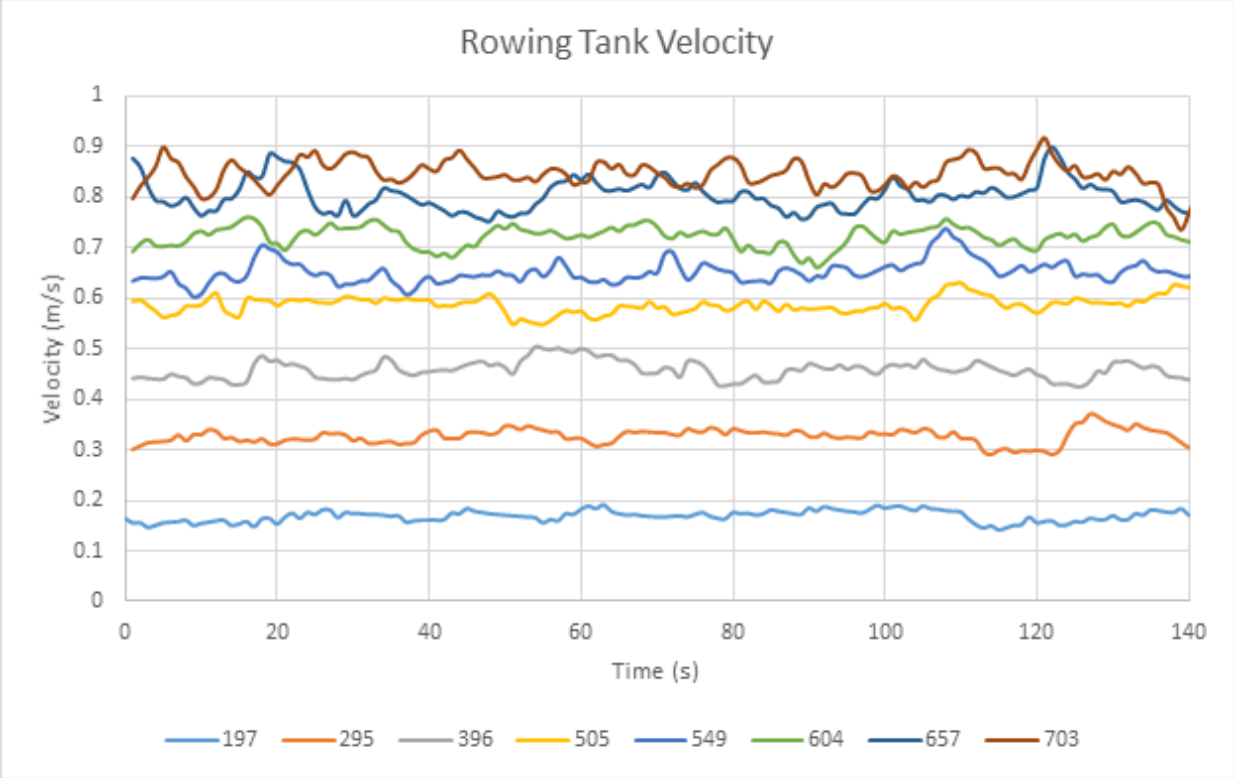

Figure 31: Water Velocities at Rowing Tank Settings

Tank settings were measured from 200 to 500 at intervals of 100, then from 550 to 700 at intervals of 50. The flow appears to become more erratic as the tank speed increases. The quickest settings, 657 and 703, even intersect each other. Figure 32 shows that the actual water velocity increased linearly as the tank setting was increased.

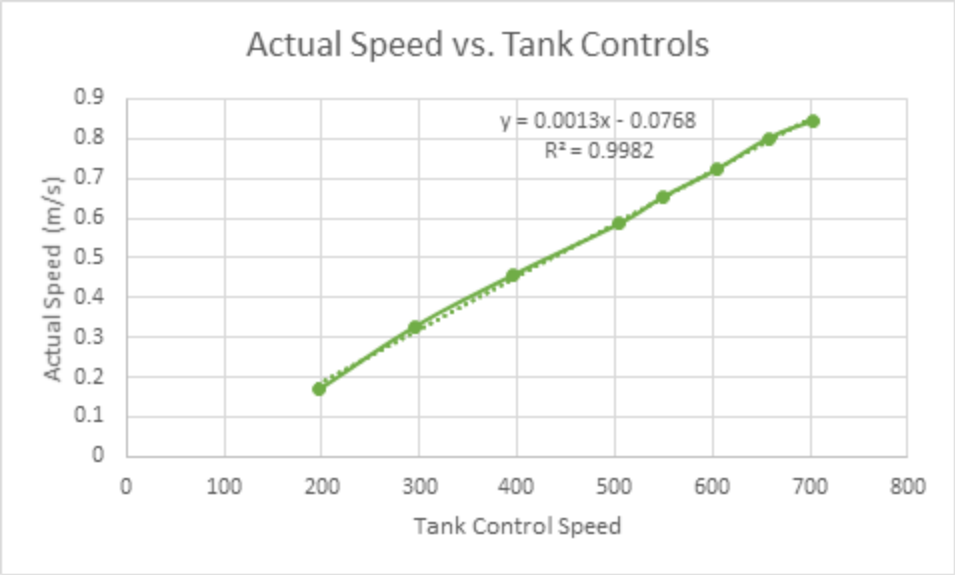

Figure 32: Average Measured Velocity vs Tank Control Speed

Prototype testing was performed at tank settings of 550 to 650. The actual water velocity of this range is 0.65 m/s to 0.80 m/s.

As observed in Figure 31, the water velocity appears to become more erratic as the magnitude increases. Figure 33 shows the minimum to maximum velocity range of the tank settings.

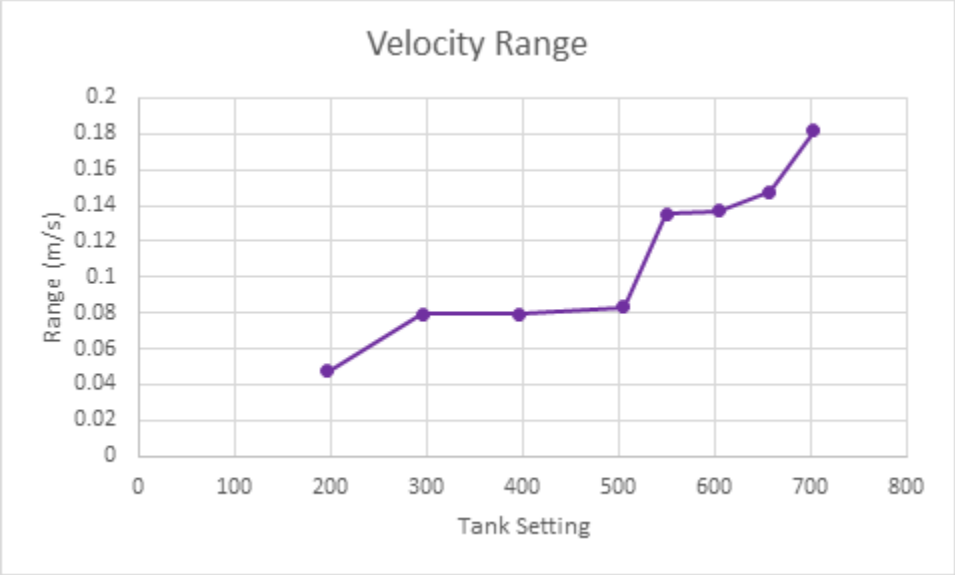

Figure 33: Velocity Range at Different Tank Speed Settings

At speed settings below 550, the velocity range is almost negligible. However, at speeds above 550 the velocity range approaches almost 0.2 m/s, or a 30% variance in water velocity. This demonstrates that the flow becomes more erratic as the water velocity increases. Prototype

testing was conducted at speed settings above 550.

During testing, the prototype would oscillate when initially placed in the rowing tanks and after a period of time would cease to oscillate. It was hypothesized that the tank speed could increase gradually, eventually knocking the water velocity out of the synchronization region. In order to determine if there is a gradual change in water velocity over an extended period of time, the actual velocity of the tank was recorded for 10 minutes. Figure 34 shows the results at a tank control setting of 604.

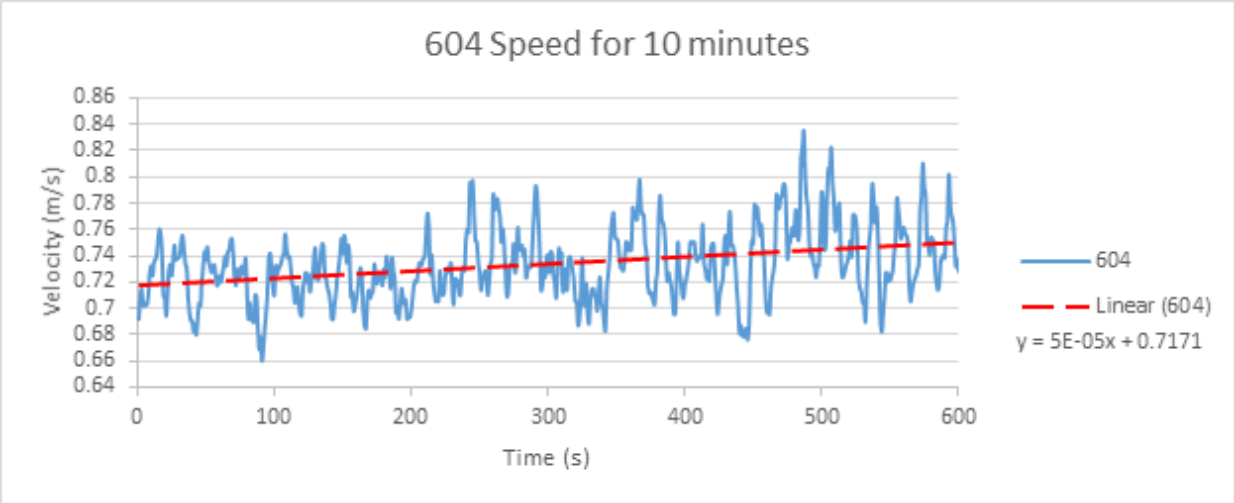

Figure 34: Water Velocity over Time at a Constant Tank Setting

The linear fit of the graph shows a very slight increase in water velocity over time. However, this average increase only makes a difference of 0.03 m/s. In order to be outside of the synchronization region, the reduced velocity must have a value less than 4 or greater than 8. For the cylinder used, that equates to a water velocity below 0.45 m/s or above 0.90 m/s. From the graph, an increase in velocity range is also observed over time. The widening range in velocity, together with the gradual increase in average speed, results in velocity spikes over 0.80 m/s starting at around 480 seconds, or 8 minutes of run time. A water velocity above 0.80 m/s pushes the reduced velocity to a value of 7. While this particular test did not go completely out of the synchronization region, water velocities recorded during energy harvester testing peaked up to 1.2 m/s, which is way out of the synchronization region. Therefore, the peak velocities after an extended period of time could have caused the oscillations to stop.

5.2 Energy Harvester Power Output

5.2.1 Voltage and Power Output

The final energy harvester prototype successfully produced 0.1 microwatts of power. However, it was not able to produce power continuously for more than about a minute because of the intermittency of the oscillations. Table 10 shows the voltage and power output of the oscillator at two different flow speeds. The load resistance for these tests was held constant at 10 MΩ.

Table 10: Power Output

Flow Speed Setting	Average Water Velocity (m/s)	Average Voltage (V)	Peak Voltage (V)	Average Power (µW)	Maximum Power (µW)
605	0.75	0.80	1.01	0.06	0.10
500	0.78	0.56	1.00	0.03	0.10

Table 10 shows that the average power output was greater at the higher flow speed setting while the maximum power output was the same for both tests. Although the second test was conducted at a lower speed setting, the actual average velocity for both tests was approximately the same. As discussed in Section 5.1, this is likely because the average water velocity increased over time. Additionally, due to the variability of the oscillations, the voltage produced by the energy harvester varied significantly over time. As seen in Figure 35, over a 30 second period the voltage varied from a minimum of 0.37 V to a maximum of 1.0 V. The water velocity during this test was also highly variable, ranging from 0.6 m/s to 1.2 m/s with an average of 0.78 m/s. However, a clear correlation between flow speed fluctuations and the changes in the voltage was not observed.

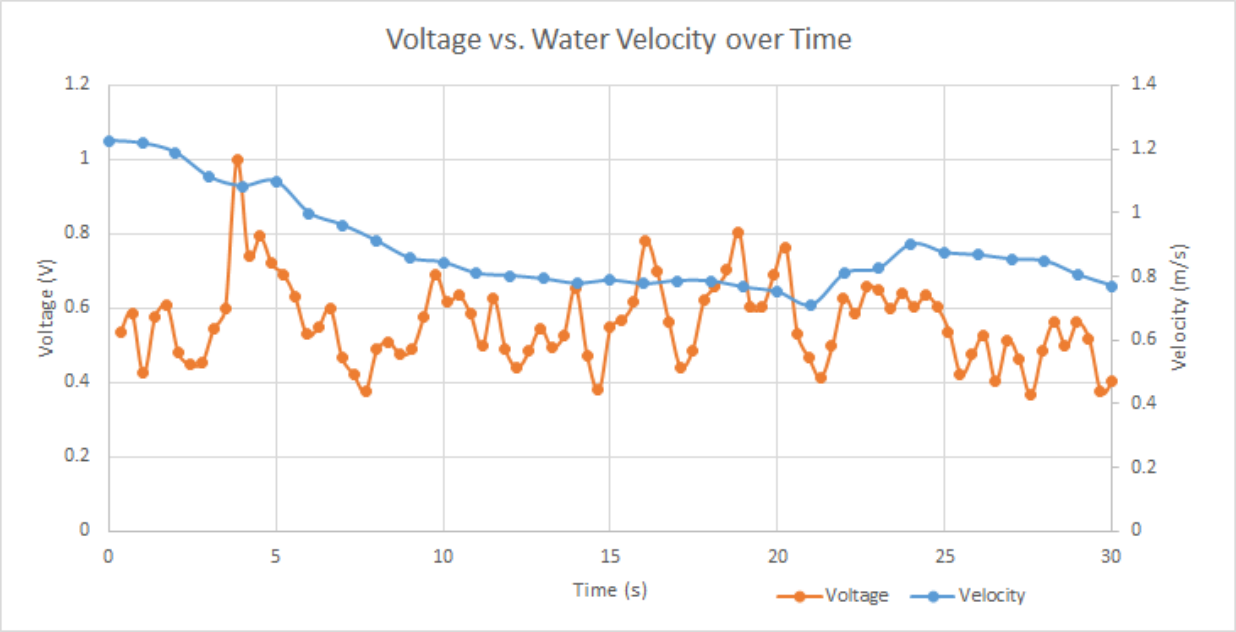

Figure 35: Voltage and Water Velocity

The inconsistency of the oscillations made it difficult to collect data over a larger range of flow speeds and load resistances. Nonetheless, these tests demonstrated that when oscillations did occur the energy harvester prototype could generate power.

5.2.2 Efficiencies

The theoretical power in the water flowing over the cylinder was determined by multiplying the force of the fluid flow on the cylinder by the water velocity using the following equation:

$$P_{fluid} = \frac{1}{2}\rho U^3 DL$$

Equation 22

For our final design, taking the average fluid velocity to be 0.6 m/s, the maximum power available from the fluid flow is 0.66W. The mechanical power of the cylinder as it oscillates was calculated using Equation 21, and was equal to 0.19W. This gives a conversion efficiency for the oscillator of 28.8%. This mechanical conversion efficiency is comparable to the experimental efficiencies obtained by previous MQPs (Hall-Stinson, Lehrman, & Tripp).

The conversion efficiency of the piezoelectrics was calculated by dividing the electrical power output of the piezoelectrics by the mechanical power of the oscillator. For the 0.1 μW maximum output of the piezoelectrics this gives an electrical conversion efficiency of

0.000053%. The overall conversion efficiency of the energy harvester is the product of the mechanical and electrical efficiencies and is equal to 0.000015%. From these results it can be seen that the low efficiency of the harvester was primarily driven by the use of film piezoelectrics as the electrical conversion method.

5.3 Resistance Testing

The resistance power curve shows where the power is at a maximum based on altering the load resistance. This means that the resistance of the external changeable load is equivalent to the internal resistance of the combination of mechanical and electrical as a whole. This value will change for each unique system design and should be tested again if further adjustments are made in the future.

Our original intent was to perform this portion of the testing with the full working prototype; however, complications with intermittency prevented this. We decided to investigate the power resistance curve with artificial forced oscillations using an oscilloscope.
Since the cylinder was oscillated by hand, it was impossible to maintain a consistent amplitude between all of the resistance loads. If an apparatus were able to maintain a consistent amplitude, the power curve would likely have greater accuracy.

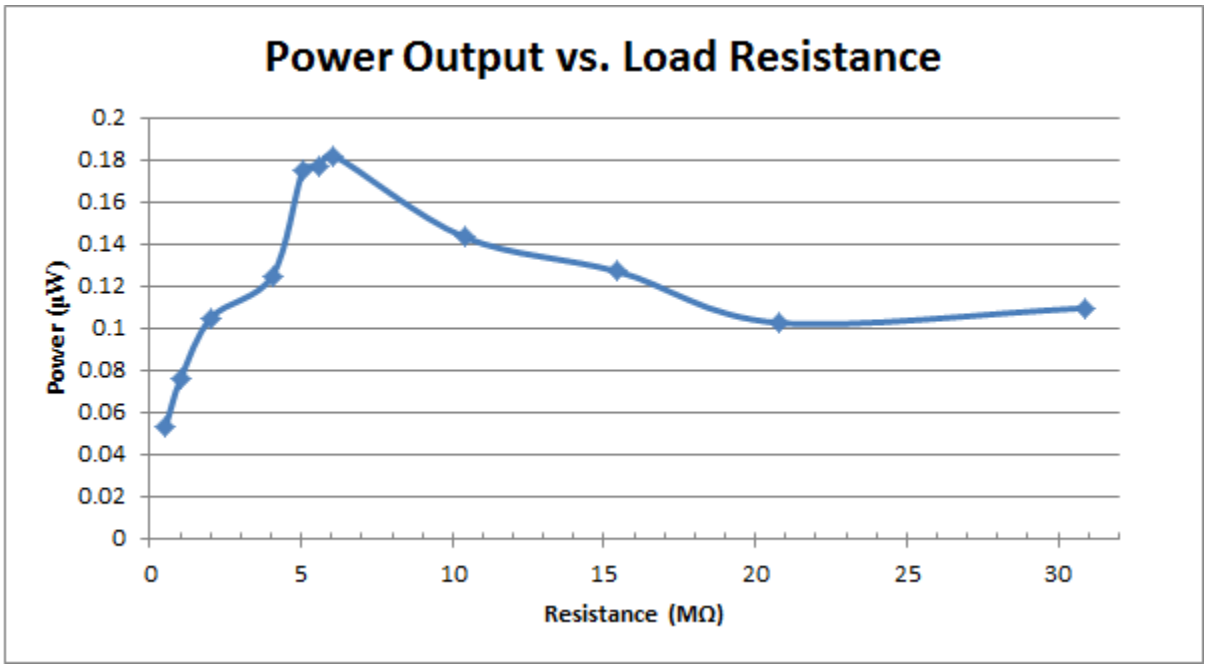

Figure 36: Power Output vs Load Resistance

The resistance that yielded the maximum power was at 6.06 MΩ with a power output of 0.187 μW. Therefore the internal resistance of the entire system would be around 6 MΩ. From Figure 36 it can be seen that the maximum values hover between 5.1 and 6.1 MΩ. Due to the issues with maintaining consistent amplitude, this reported maximum resistance may shift within this range. The theoretical efficiency is also at 50% of its maximum at this point, meaning that higher efficiencies are possible at greater resistance values, but it was decided to focus on the maximum power output rather than the maximum efficiency.

6. Conclusions and Recommendations

6.1 Oscillations

The oscillator prototype successfully vibrated in flowing water, with amplitudes up to 1.2cm and frequencies up to 3.2 Hz. The oscillator's behavior was effectively predicted by the linear harmonic oscillator model. For a water velocity of 0.58 m/s the measured amplitude was within 2mm of the predicted amplitude and the frequency was within 1.0 Hz.

As seen in Table 9 in Section 3.4.4.2, the amplitude and frequency for the physical prototype were both consistently lower than predicted. The lower amplitude can be attributed to several factors. First, the damping for this prototype had to be estimated instead of measured, so it was likely higher than the 0.1 damping value used in calculations. Second, the linear harmonic model assumes a constant lift coefficient 0.5, when in practice the lift coefficient varies over time. Additionally, the proximity of walls increases the drag coefficient and decreases the lift coefficient (Techet, 2005). Since the oscillator was close to the bottom and side wall of the rowing tanks, the average lift coefficient was likely lower than 0.5. The lower frequency can also be attributed to higher damping and wall effects. However, overall the linear harmonic model provided an accurate prediction of VIV behavior.

6.2 Power Generation

The energy harvester was able to successfully generate power from the cylinder oscillations. This was achieved by connecting the piezoelectric directly to the springs in series as opposed to in parallel, where the combined spring constant of the system was far too high to allow for both power generation and consistent oscillations. Connecting the piezoelectrics and springs in series resulted in a negligible increase in combined spring constant, though the force exerted on the piezoelectrics, and therefore the power generated, was less than that of the parallel attachment.

6.3 Efficiency

While the 28.8% mechanical efficiency of the oscillator was in the expected range for VIV, the efficiency of the energy harvester was very low due to the use of film piezoelectric transducers. PVDF film piezoelectrics were chosen because they could be used for the small scale of our prototype. However, the low conversion efficiency of the piezoelectrics was

expected because of the low oscillation frequency of the system. Piezoelectrics can reach efficiencies up to 90% when oscillated near their own natural frequency, but the efficiency decreases dramatically as the system frequency moves away from the natural frequency of the piezoelectric (Sherrit, 2008). The natural frequency of the transducers used in this project was approximately 1 kHz, while the maximum frequency reached by the oscillator was 3.2 Hz. This large difference in frequency explains why the electrical conversion efficiency of the energy harvester was only 0.000053%.

The efficiency of the system could be improved by increasing the frequency of the oscillations or choosing a piezoelectric with a lower natural frequency. However, the frequency of the oscillations is limited by the water velocity, so it could not feasibly be increased to the kHz range. Similarly, film piezoelectrics do not generally have frequencies less than 1 kHz, so it would be difficult to change. Ceramic piezoelectrics can have natural frequencies as low as 1 Hz, so it could be possible to create a more efficient harvester by incorporating ceramic transducers instead of film. To further improve efficiency on a larger scale, it would be more practical to switch to different electrical conversion methods such as electromagnetic or electrostatic.

6.4 Intermittent Oscillations

VIV was able to occur sporadically in the energy harvesting system. However, the oscillations of the cylinder were intermittent and irregular, which prevented consistent measurement. As mentioned in Section 5.1, the velocity of the water in the rowing tanks was erratic, especially at higher speeds. Over an extended time, there were spikes in water velocity above 0.80 m/s, which pushed the reduced velocity out of synchronization range. These repeated spikes made continuous oscillation very difficult to achieve.

The rowing tank water velocity is shown in Figure 37. Blue indicates low flow speed while red indicates a faster flow speed of 0.9 m/s. The oscillating cylinder was placed at nearly center depth, seen in Figure 37 as orange, or about 0.75 m/s. The edges of the tank had a slower flow speed and the sloped side of the tank created some speed variation in the center. This made it extremely difficult for the oscillator prototype to be placed in an area with a consistent flow speed.

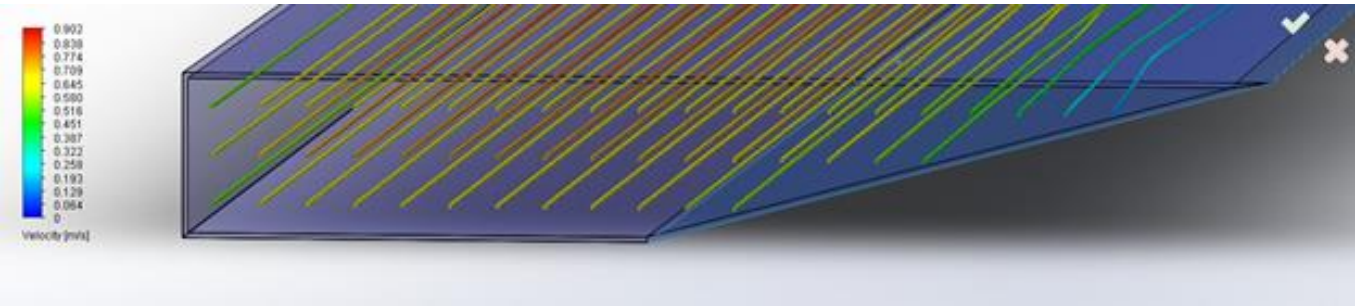

Figure 37: Simulated Rowing Tank Water Velocity Profile

In addition to the varied flow speed caused by the profile of the rowing tank, the shallow depth of the tank created some difficulties. The oscillator prototype was relatively close to the surface of the water which led to waves and surface effects influencing the consistency of the oscillations. One possible way to determine the influence of the surface and wave effects was analyzing the Froude number of the rowing tank waves. If the Froude number for the waves went from subcritical (Fr < 1) to supercritical (Fr > 1), then the flow behavior would change, which could explain the intermittent oscillations. The Froude number for waves in shallow water is given by Equation 23, where U is the fluid velocity, g is gravitational acceleration, and d is the depth of the water.

$$\mathrm{Fr} = \frac{U}{\sqrt{gd}}.$$

Equation 23

For the rowing tanks, when the water is at a depth of 34.3 cm, the Froude number ranges from 0.27 to 0.82 at water velocities of 0.5 m/s and 1.5 m/s respectively. This demonstrates that the flow was in the subcritical Froude number range during our testing. In order for the flow to become critical (Fr = 1) at this water depth, the water velocity would have to reach 1.8 m/s. This velocity value is above what we observed in the tank, which shows us that the flow was subcritical for the entirety of our testing. This rules out supercritical flow as an explanation for the intermittent oscillation.

6.5 Recommendations for Future Testing (Small Scale)

Although we were unable to achieve consistent VIV oscillations, there is still opportunity for continued testing and research since the theory is still sound. For future testing,

there are a couple of improvements that can be made in order to increase the chances of success. The most significant improvement moving forward would be to find a testing facility with a more consistent flow. Our project was limited and constrained by the inconsistent flow speed, which prevented us from fully testing the parameters of our energy harvesting design.

If a more controlled and consistent testing facility can be utilized, then there are additional tests that can be conducted to determine the optimal piezoelectric energy harvester system. For example, the mass of the system can be varied in order to get the natural frequency of the device as close as possible to the vortex shedding of the water. Testing over a wider range of water velocities can also be conducted in order to determine how large a range the oscillations can occur in. In addition, the load resistance test that our team conducted out of the water can be conducted in the water to truly determine the optimal load resistance.

Another parameter of the energy harvester design that can be tested is to increase the number of piezoelectric transducers attached in series. Our design had two transducers attached in series, but adding more, in theory, would increase the voltage produced in the system. This would help increase the amount of power generated and could potentially increase the efficiency of the energy harvester. However, a more secure method of attaching the piezoelectric films to the springs should be investigated to improve durability.

6.6 Large Scale Testing and Real World Feasibility

To determine if VIV is a practical harvesting method, testing needs to be conducted on a larger scale than the energy harvester constructed for this project. Testing on a larger scale would allow for a better determination of how much power could actually be generated using VIV. It would reduce the effects of variables such as friction, boundary layer effects, and erratic flow speed which had a significant impact on the consistency of our prototype. Additionally, increasing the scale of the project would allow for the use of more efficient electrical conversion methods such as electromagnetic or electrostatic.

For a linear alternator, which converts linear oscillation into electrical power using electromagnetism, the mechanical to electrical efficiency could realistically be 95% (Bard & Kracht, 2013). Based on the 28.8% mechanical conversion efficiency measured in this project, a device using a 95% efficient linear alternator could feasibly produce 1 kW of electrical power in

water flowing at 0.6 m/s. Assuming appropriate springs could be chosen based on the system mass, this could be accomplished by using 20 cylinders with a diameter of 0.45m and a length of 3.44m.

Large scale VIV energy harvesting has the potential to produce a greater amount of power with more consistency than the small scale harvester used in this project. However, as the size of the harvester increases, it has a greater impact on the environment. In order for VIV to become an environmentally friendly hydropower alternative, the size of the harvester must be limited, which would limit its power production.

References

Accelerometers: Introduction to Acceleration Measurement. (2016). Omega.

American Shad. (n.d.). Retrieved October 12, 2016, from http://www.wildlife.state.nh.us/fishing/profiles/american-shad.html

Avram, P., McKee, R., Tuzun, T., & Geiger, B. (2008). A Linear Generator Power Take-Off System for the VIVACE Hydrokinetic Energy Converter.

Ball, I. M., Killen, T. J., Sakhuja, S., Warner, E. T., & Faculty Advisor: Savilonis, B. J. (2012). Maximizing Vortex Induced Vibrations through Geometry Variation.

Bard, J., & Kracht, P. (2013). Report on Linear Generator Systems for Wave Energy Converters. Structural Design of Wave Energy Generators.

Bernitsas, M. M., Ben-Simon, Y., Raghavan, K., & Garcia, E. M. (2008). The VIVACE Converter: Model Tests at High Damping and Reynolds Number Around 105. Journal of Offshore Mechanics and Arctic Engineering, 131(1), 011102-011102. doi:10.1115/1.2979796

Bearman, P. W. (1984). Vortex Shedding from Oscillating Bluff Bodies. Annual Review of Fluid Mechanics, 16(1), 195-222. doi:10.1146/annurev.fl.16.010184.001211

Boisseau, S.,Despesse, G. and Seddik, B. Ahmed. Electrostatic Conversion for Vibration Energy Harvesting, Small-Scale Energy Harvesting, Intech, 2012.

Blevins, R. (1990). Flow-Induced Vibration. New York: Van Nostrand Reinhold.

Costanzo, I., Kelsey, A., Ogren, F., Wians, D., & Faculty Advisor: Savilonis, B. J. (2016). Design of a Novel Concept for Harnessing Tidal Stream Power.

Distler, D. B., Johnson, B. G., Kielbasa, M. J., Phinney, B. C., & Faculty Advisor: Savilonis, B. J. (2011). Optimization of Oscillating Body for Vortex Induced Vibrations.

Dynamometer: Introduction and Types. (2015).

Elert, G. (2002). Speed of Ocean Currents. Retrieved September 21, 2016, from http://hypertextbook.com/facts/2002/EugeneStatnikov.shtml

Effects on the Environment. (2015). Retrieved October 12, 2016, from http://nnmrec.oregonstate.edu/education/effects-environment

Environmental Impact of Wave Energy Devices. (n.d.). Retrieved October 12, 2016, from http://www.alternative-energy-tutorials.com/energy-articles/environmental impact-of-wave-energy.html

Flahiff, D. (2008, December 3). VIVACE: Slow Water Current Energy Mimics Schools of Fish. Retrieved September 21, 2016, from http://inhabitat.com/vivace-vortex-hydro-energy/

Hall-Stinson, A. S., Lehrman, C. J., Tripp, E. R., & Faculty Advisor: Savilonis, B. J. (2011). Energy Generation from Vortex Induced Vibrations.

Gabbai, R. D., & Benaroya, H. (2005). An overview of modeling and experiments of vortex-induced vibration of circular cylinders. Journal of Sound and Vibration, 282(3–5), 575-616. doi:http://dx.doi.org/10.1016/j.jsv.2004.04.017

Hadas, Z., Ondrusek, C., & Singule, V. (2010). Power sensitivity of vibration energy harvester. Microsystem technologies, 16(5), 691-702.Pranita, B. A. (2016). Subsea Pipeline: Fatigue Free Span Analysis.

Hobbs, W. B. (2010). Piezoelectric energy harvesting: vortex induced vibrations in plants, soap films, and arrays of cylinders.

Kuhn, A. (2008, January 3). Relocated Three Gorges Residents Face Challenges. Retrieved October 12, 2016, from http://www.npr.org/templates/story/story.php?storyId=17784497

Measurement Specialties. “Piezo Film Sensors Technical Manual.” Retrieved from https://www.sparkfun.com/datasheets/Sensors/Flex/MSI-techman.pdf

Measurement Specialties (2009). “DT Series Elements with Lead Attachment Data Sheet.” Retrieved from http://www.mouser.com/ds/2/418/DT_Series_LeadAttach-709992.pdf

Mehmood, A., Abdelkefi, A., Hajj, M. R., Nayfeh, A. H., Akhtar, I., & Nuhait, A. O. (2013). Piezoelectric energy harvesting from vortex-induced vibrations of circular cylinder. Journal of Sound and Vibration, 332(19), 4656-4667. doi:http://dx.doi.org/10.1016/j.jsv.2013.03.033

Modir, Alireza, Kahrom, Mohsen & Farshidianfar, Anoshirvan. Mass ratio effect on vortex induced vibration of a flexibly mounted circular cylinder, an experimental study, International Journal of Marine Energy, Volume 16, December 2016, Pages 1-1

Piezo Systems. “Piezoceramic Materials and Properties.” Retrieved from http://www.piezo.com/prodmaterialprop.html

Principles of Strain Gauges. Kyowa.

LVDT Pressure Sensors. (2009). Sensorland.

Ledoux, A. (2011). Theory of Piezoelectric materials and their Applications in Civil Engineering (Doctoral dissertation, Massachusetts Institute of Technology).

Maximum Power Transfer Theorem. (2015, April 21). Retrieved September 22, 2016, from http://www.electronicshub.org/maximum-power-transfer-theorem/

See, L. (2003, June 08). Waters of Three Gorges Dam Will Wash Over World Culture. Retrieved October 12, 2016, from http://articles.latimes.com/2003/jun/08/opinion/oe-see8

Sherrit, S. (2008). The Physical Acoustics of Energy Harvesting. Pasadena, CA: Jet Propulsion Labratory, California Institute of technology.

Tardiveau, R., Giraud, F., Amanci, A., Dawson, F., Giraud-Audine, C., Amberg, M., & Lemaire-Semail, B. (2013). Power Consideration in a Piezoelectric Generator. Smart Materials Research, 2013.

Techet, A. H. (2005). Vortex Induced Vibrations: MIT Opencourseware. Shu, Y.C., and Lien, I.C. (2006). Analysis of Power Output for Piezoelectric Energy Harvesting Systems. Smart Materials and Structures. 15, 1499.

The Strain Gauge. (2016). Omega.

Umans, S. D., & .. (n.d.). Fitzgerald and Kingsley's Electric Machinery.

University Communications. (2013, January 16). Hydropower Dams Hamper Migrating Fish Despite Passage Features, Study Finds. Retrieved October 12, 2016, from https://uanews.arizona.edu/story/hydropower-dams-hamper-migrating-fish-despite-passage-features-study-finds

U.S. Energy Information Administration (2016). Retrieved from http://www.eia.gov/

Vortex Hydro Energy. (2016). Retrieved from http://www.vortexhydroenergy.com

Wagner, Jürgen (Self-photographed) [CC BY-SA 4.0 (http://creativecommons.org/licenses/bysa/4.0)], via Wikimedia Commons

Williamson, C. H. K., & Govardhan, R. (2008). A brief review of recent results in vortex-induced vibrations. Journal of Wind Engineering and Industrial Aerodynamics, 96(6–7), 713-735. doi:http://dx.doi.org/10.1016/j.jweia.2007.06.019

Williamson, C.H.K. & Govardhan, R. (2004). Vortex-Induced Vibrations. Annual Review of Fluid Mechanics, 36(1), 413-455. doi:doi:10.1146/annurev.fluid.36.050802.122128

Zahari, M. A., & Dol, S. S. (2014). Application of Vortex Induced Vibration Energy: Generation Technologies to the Offshore Oil and Gas Platform: The Preliminary Study (Vol. 8): International Journal of Mechanical, Aerospace, Industrial, Mechatronic and Manufacturing Engineering.

Zhang, Min & Wang, Junlei, "Experimental Study on Piezoelectric Energy Harvesting from Vortex-Induced Vibrations and Wake-Induced Vibrations," Journal of Sensors, vol. 2016, Article ID 2673292, 7 pages, 2016. doi:10.1155/2016/2673292

Appendix A: Materials List

Item	Quantity
¼-in width PVC sheet, 15in x 8in	2
¼-in width PVC sheet, 4in x 14in	2
25in x 1in shelving bracket	2
1in corner brace	12
#8 0.5in long screw	32
#8 3.5in long machine screw	2
#8 nut	38
#8 washer	34
#8 1.5in eye bolt	2
Steel wire extension springs, 0.24 lb/in	2
Piezoelectric film transducer	2
¾-in PVC cylinder	1
¾-in PVC cylinder end cap	2
Epoxy	1 container
2in corner brace	4
1.5in corner brace	2
¼-in 5in long machine screw	2
¼-in 1in long machine screw	4
¼-in nut	10
¼-in 1.5in long wood screw	12
¼-in 2.5in long wood screw	4
10in mending plate	2
2 x 4 wooden plank, 110in long	2

Item	**Quantity**
¼-in width PVC sheet, 15in x 8in	2
¼-in width PVC sheet, 4in x 14in	2
25in x 1in shelving bracket	2
2 x 3 wooden plank, 18in long	1